

# Geometric Aspects and Testing of the Galactic Center Distance Determination from Spiral Arm Segments

I. I. Nikiforov\* and A. V. Veselova

*St. Petersburg State University, Universitetskii pr. 28,  
Staryi Peterhof, St. Petersburg, 198504 Russia*

**Abstract**—We consider the problem of determining the geometric parameters of a Galactic spiral arm from its segment by including the distance to the spiral pole, i.e., the distance to the Galactic center ( $R_0$ ). The question about the number of points belonging to one turn of a logarithmic spiral and defining this spiral as a geometric figure has been investigated numerically and analytically by assuming the direction to the spiral pole (to the Galactic center) to be known. Based on the results obtained, in an effort to test the new approach, we have constructed a simplified method of solving the problem that consists in finding the median of the values for each parameter from all possible triplets of objects in the spiral arm segment satisfying the condition for the angular distance between objects. Applying the method to the data on the spatial distribution of masers in the Perseus and Scutum arms (the catalogue by Reid et al. (2014)) has led to an estimate of  $R_0 = 8.8 \pm 0.5$  kpc. The parameters of five spiral arm segments have been determined from masers of the same catalogue. We have confirmed the difference between the spiral arms in pitch angle. The pitch angles of the arms revealed by masers are shown to generally correlate with  $R_0$  in the sense that an increase in  $R_0$  leads to a growth in the absolute values of the pitch angles.

Keywords: *spiral structure, solar Galactocentric distance, maser sources, spatial distribution, Galaxy (Milky Way).*

---

\*E-mail: nii@astro.spbu.ru

## 1. INTRODUCTION

Studies of the observed manifestations of the spiral structure of galaxies, which give initial constraints for constructing the theories of its formation, are of fundamental importance for galactic astronomy and stellar dynamics. Such studies for our Galaxy can potentially give the most detailed information. However, they are complicated by the observation of the spiral structure "edge-on" due to the location of the Sun near the disk plane, by the fact that only the local Galactocentric sector is well studied, by the extinction in the disk, by the shielding of the region behind the Galactic center, by the low accuracy or the absence of data on the heliocentric distances for spiral pattern tracers, and by other difficulties. There exist two classes of methods for studying the Galactic spiral structure: (1) based on the spatial distribution of tracers of various features of this structure and (2) based on the kinematics of such tracers (for more details see, e.g., Niki-forov and Shekhovtsova 2001). Each of the classes has its advantages and disadvantages. The kinematic approach in the case of tying to the dynamical perturbations from the spiral pattern can produce well-conditioned parametric models, but it requires additional assumptions (in particular, about the nature of the spiral arms) that may turn out to be inadequate. The spatial approach has no need for such assumptions and is applicable to any features of the spiral structure irrespective of their nature, but reliable results from an analysis of the spatial distribution may be expected only for those types of tracers by which these features are identified unambiguously.

Until recently, any spatial modeling of the Galactic spiral structure has been based predominantly on the data on tangential and other concentrations of gas and objects tracing the spiral arms in an attempt to "assemble" a regular structure from these individual segments while guided by not so much by the geometry of individual concentrations as by their positions (Efremov 2011). Of course, this can be done only under some assumptions. Not always, but usually, the following was assumed in such modeling: (1) the arms have the shape of a logarithmic spiral; (2) the spiral pitch angle ( $i$ ) is constant; (3) the angle  $i$  is the same for all arms; (4) the number of arms in the Galaxy is specified (as a rule, two or four, both variants were occasionally considered), which largely defines the pitch angle; (5) the pole of the spiral arms lies at the Galactic center; and (6) the solar Galactocentric distance ( $R_0$ ) is taken to be fixed. Heterogeneous, including not very reliable, estimates of the heliocentric distances with a large fraction of kinematic distances, especially for distant structural features, were often used in this case. The problem is also complicated by the fact that the objects that, in principle, gravitate toward the spiral arms also populate the interarm space.

Obviously, due to these difficulties and, possibly, the inadequacy of the assumptions made, it is impossible to obtain unambiguous results within this approach. For example, Efremov (2011) concluded that in the inner Galaxy ( $R < 9 - 10$  kpc) a four-armed spiral pattern with  $i = 10^\circ - 12^\circ$  is in better agreement with the data on the distribution of neutral, molecular, and ionized hydrogen. By contrast, Francis and Anderson (2012) conclude that the distribution of H I, giant molecular clouds, H II regions, and 2MASS sources corresponds to a two-armed logarithmic spiral with  $i \sim 5.5^\circ$  (also in the inner

Galaxy,  $R < 12 - 15$  kpc). Pohl et al. (2008) also preferred a two-armed model, but with  $i \sim 12^\circ$ , to represent the CO data, while abandoning, however, the reproduction of some features in the constructed molecular gas distribution by the model.

At the same time, an alternative approach is possible — the spatial modeling of a *separate* arm segment or several arm segments *separately*. In particular, this makes it possible to determine the segment pitch angles without the assumption (number 4 in our list) about the number of arms in the Galaxy. Such an analysis was undertaken by Pavlovskaya and Suchkov (1984), Avedisova (1985), Dame et al. (1986), Vallée (1988), and Grabelsky et al. (1988), but the development of this approach was restrained by a shortage of reliable distance estimates, especially for tracers with a strong concentration to the spiral arms.

The situation is changed noticeably by the recent appearance of databases that allow one to produce samples of spiral pattern tracers that (1) are strongly concentrated to the spiral arms, (2) have at least internally accurate heliocentric distances, and (3) allow the arm segments to be traced over a length long enough to reveal their geometry (preferably the curvature). Samples with such properties are available at least for masers with trigonometric parallaxes (see, e.g., Reid et al. 2014) and young open clusters (see, e.g., Popova and Loktin 2005; Nikiforov and Kazakevich 2009).

An analysis of the spatial distribution of tracers based on new data aimed at determining the geometric parameters of individual spiral segments has already been performed by a number of research groups. Popova and Loktin (2005) estimated the pitch angle of spiral arms based on data from the Homogeneous Catalogue of OSC parameters without using assumption 4 but assuming the pitch angles to be identical for all segments (assumption 3 in our list). Reid et al. (2009, 2014), Xu et al. (2013), and Bobylev and Bajkova (2013, 2014) performed the corresponding modeling for masers with trigonometric parallaxes by abandoning both assumptions 3 and 4. Note that when investigating the nature of the Local arm (Xu et al. 2013), which implies finding the parameters of precisely this feature, the statement of the problem itself requires abandoning assumption 3.

A similar analysis for classical Cepheids is more problematic due to their generally less pronounced concentration to the spiral arms. Popova (2006) and Dambis et al. (2015) applied the procedures for identifying the objects belonging to the ridelines of spiral segments to obtain more stable results from Cepheids (note that Popova and Loktin (2005) also used the same procedure for open clusters). On the other hand, the more disperse distribution of Cepheids is partly compensated for by the high internal accuracy of their distance estimates and the large size of their present-day samples. In both papers the results were obtained without assumption 4, while in Dambis et al. (2015) assumption 3 was also abandoned.

If it is assumed that with the currently available data the spatial modeling of spiral segments allows their geometry to be established with confidence (in particular, the pitch angle to be determined) without relying on assumptions 3 and 4, then one can attempt to go even further and to free the parameter  $R_0$ , i.e., to abandon assumption 6. This

will make it possible to model the spiral segments more completely, because from general considerations one might expect the existence of a significant dependence of the pitch angles on  $R_0$  (as confirmed by our calculations). Furthermore, this can give a new method of determining the distance to the Galactic center as the distance from the Sun to the pole (geometric center) of the spiral structure. The proposed method can become the first spatial method of determining  $R_0$  applicable to objects of the flat Galactic subsystem. The method can be both absolute, when using the data on masers with trigonometric parallaxes, and relative, if it is applied to objects with photometric distances (for the classification of  $R_0$  measurements, see the review by Nikiforov (2004)). In principle, the method can be applied to any objects tracing the Galactic spiral structure.

A rigorous consideration of this problem by taking into account two uncertainties (the scatter across the arm and the random errors in the heliocentric distances) will possibly allow some other assumptions from the above list to be additionally abandoned. However, the rigorous method suggests laborious calculations even in the variant being considered here (when abandoning only assumptions 3, 4, and 6). Therefore, first of all, we should check whether the new approach is operable in principle both for the currently available data and in prospect. In this paper we initially consider the idealized (geometric) problem of reconstructing the parameters of a logarithmic spiral as a figure from points belonging to it by assuming that the direction to the spiral pole (Galactic center) is known (Section 2). Then, to test the proposed approach, we construct a simplified method of solving the problem for real data and apply it to masers (Section 3). The simplified method is tested through numerical simulations in Section 4. The method and results obtained are discussed in Section 5.

## 2. THE PROBLEM OF DETERMINING THE PARAMETERS OF A LOGARITHMIC SPIRAL FROM POINTS OF ITS SEGMENTS

### *2.1. The Formulas to Determine the Parameters of a Spiral from Three Points*

Consider the geometric problem on the possibility of reconstructing the parameters of a logarithmic spiral from points belonging to its segment. We will assume the spiral to be in the Galactic plane and the direction from the Sun to the spiral pole (to the Galactic center) to be known. The separate Galactic arm will then be represented by a segment of the logarithmic spiral

$$R(\lambda) = |R_0|e^{k(\lambda-\lambda_0)}. \quad (1)$$

Here,  $\lambda \in (-\infty, +\infty)$  is the Galactocentric longitude (measured from the sunward direction clockwise when viewed from the North Galactic Pole, i.e., in the direction of Galactic rotation);  $k \equiv \tan i$ , where  $i$  is the pitch angle (negative for a trailing spiral);  $\lambda_0$  is the position parameter ( $R(\lambda_0) = |R_0|$ ). In the sunward direction  $\lambda = 0 \pm 2\pi n, n \in \mathbb{Z}$ .

Since the logarithmic spiral is specified by Eq. (1) containing three parameters  $(R_0, k, \lambda_0)$ , let us consider the possibility of determining these parameters from three (different) points  $M_1(r_1, l_1, b_1)$ ,  $M_2(r_2, l_2, b_2)$ , and  $M_3(r_3, l_3, b_3)$  lying on one spiral turn when

projected onto the Galactic plane. Here,  $r_j$ ,  $l_j$ , and  $b_j$  are, respectively, the heliocentric distance, Galactic longitude and latitude of point  $M_j$ ,  $j = 1, 2, 3$ . Let us assume that  $\lambda_1 < \lambda_2 < \lambda_3$ ; the Galactocentric longitudes of such points then satisfy the inequality

$$\lambda_3 - \lambda_1 < 2\pi. \quad (2)$$

Formula (1) gives the expressions for the Galactocentric distances  $R_j$  of points  $M_j$  via the corresponding Galactocentric longitudes:

$$R_j = |R_0| e^{k(\lambda_j - \lambda_0)}, \quad j = 1, 2, 3. \quad (3)$$

On the other hand,  $R_j$  can be found from the coordinates  $r_j$ ,  $b_j$ , and  $l_j$  of points  $M_j$  depending on the spiral parameter  $R_0$ :

$$R_j = \sqrt{R_0^2 + r_j^2 \cos^2 b_j - 2R_0 r_j \cos l_j \cos b_j}, \quad j = 1, 2, 3. \quad (4)$$

Passing to the Cartesian coordinates

$$X_j = r_j \cos l_j \cos b_j, \quad Y_j = r_j \sin l_j \cos b_j, \quad Z_j = r_j \sin b_j, \quad (5)$$

we will write the following expressions for the Galactocentric longitudes:

$$X_j = R_0 - R_j \cos \lambda_j, \quad Y_j = R_j \sin \lambda_j. \quad (6)$$

Formulas (5) and (6) show that at fixed  $r_j$ ,  $b_j$ , and  $l_j$  and given  $R_0$  we can unambiguously determine only the *nominal* Galactocentric longitudes  $\Lambda_j$  for points  $M_j$  such that

$$-\pi \leq \Lambda_1 \leq \Lambda_2 \leq \Lambda_3 < \pi; \quad (7)$$

$$\sin \Lambda_j = \frac{Y_j}{R_j}, \quad \cos \Lambda_j = \frac{R_0 - X_j}{R_j}, \quad j = 1, 2, 3. \quad (8)$$

The *rotational* longitudes  $\lambda \in (-\infty, +\infty)$  can differ from the nominal longitudes  $\Lambda$  by an integer number of complete rotations. The Galactocentric longitudes enter into the final formulas to calculate the spiral parameters  $R_0$  and  $k$  as the differences of the longitudes of two points belonging (by the initial assumption) to one spiral turn, which allows the rotational longitudes to be replaced by the nominal ones in the formulas.

Based on equalities (3), we will set up the following system of equations for the unknown parameters  $R_0$  and  $k$ :

$$R_1/R_2 = e^{k(\Lambda_1 - \Lambda_2)}, \quad R_2/R_3 = e^{k(\Lambda_2 - \Lambda_3)}. \quad (9)$$

Let us express  $k$ , for example, from the first equality in (9), then  $k = \ln(R_1/R_2)/(\Lambda_1 - \Lambda_2)$ , and substitute it into the second one. Taking the logarithm of the latter, we obtain the equation for  $R_0$

$$(\Lambda_3 - \Lambda_2) \ln R_1 + (\Lambda_1 - \Lambda_3) \ln R_2 + (\Lambda_2 - \Lambda_1) \ln R_3 = 0. \quad (10)$$

All quantities in (10) are functions of only  $R_0$  and the coordinates of points  $M_j$ .  $R_j$  and  $\Lambda_j$  are defined by Eqs. (4) and (8), respectively.<sup>1</sup> Equation (10) was solved numerically.

Once  $R_0$  has been found from Eq. (10), the other two spiral parameters are determined by any pair from the following expressions:

$$k = \ln(R_j/R_m)/(\Lambda_j - \Lambda_m), \quad j, m = 1, 2, 3, \quad j \neq m; \quad (11)$$

$$\lambda_0 = \Lambda_j - \frac{\ln(R_j/|R_0|)}{k}, \quad j = 1, 2, 3. \quad (12)$$

At  $k = 0$  (circumference) Eq. (10) is trivial, while Eq. (11) is meaningless. Equation (10) and expressions (11), (12) constitute the formal apparatus of the method for determining the parameters of a logarithmic spiral that we will call the *three-point* one.

## 2.2. The Number of Roots of the Three-Point Equation for the Parameter $R_0$

Since Eq. (10) is transcendental, the question about the number of its roots, i.e., the question about the uniqueness of reconstructing the parameters of a logarithmic spiral from three points belonging to one its turn, deserves a separate consideration. Let such points  $M_1$ ,  $M_2$ , and  $M_3$  belong to a spiral with parameters  $R_0$ ,  $k$ , and  $\lambda_0$ . Consider a variable  $R'_0$  that has the meaning of a trial value of  $R_0$  defining the quantities  $R_j$  and  $\Lambda_j$ ,  $j = 1, 2, 3$ . For the left-hand side of (10) we will introduce the notation

$$f(R'_0) \equiv (\Lambda_3 - \Lambda_2) \ln R_1 + (\Lambda_1 - \Lambda_3) \ln R_2 + (\Lambda_2 - \Lambda_1) \ln R_3. \quad (13)$$

At  $R'_0 = R_0$  the value of  $f(R'_0)$  is zero. But is the reverse true: does finding such  $R'_0$  that  $f(R'_0) = 0$  imply an *unambiguous* determination of the parameter  $R_0$  for the spiral passing through three points? I.e., do three points define a spiral in this statement of the problem?

Our predominantly numerical study of the behavior of  $f(R'_0)$  depending on the initial data and spiral parameters revealed basic properties of this function. Let us illustrate them using the model spirals corresponding to the outer and inner (with respect to the Sun) Galactic arms as an example.

Let the initial points  $M_1$ ,  $M_2$ , and  $M_3$  belong to one turn of the logarithmic spiral representing the Sagittarius arm with parameters  $R_0 = 8.0$  kpc and  $i = -18.7^\circ$  (Nikiforov and Shekhovtsova 2001), and  $\lambda_0 = -30^\circ$ . In what follows, we will call this spiral the *initial* one. When calculating the function  $f(R'_0)$  defined by the set of three initial points, we renumbered the latter for each value of  $R'_0$  in such a way that condition (7) was fulfilled, i.e., the numbering of points  $M_j$  at  $R'_0 \neq R_0$  might coincide or not coincide with the initial one. This ensures an increase of the point number with growing formal longitude  $\Lambda(R'_0)$  at any value of  $R'_0$  for nondegenerate configurations ( $\Lambda_j \neq \Lambda_m, j \neq m$ ). This numbering

---

<sup>1</sup>We can save on calculations using the equation  $(\Lambda_3 - \Lambda_2) \ln R_1^2 + (\Lambda_1 - \Lambda_3) \ln R_2^2 + (\Lambda_2 - \Lambda_1) \ln R_3^2 = 0$  equivalent to Eq. (10). It will then suffice to find  $R_j^2$  without taking the square root.  $R_j$  does not need to be known to find  $\Lambda_j$ .

rule and condition (7) follow from the statement of the problem of searching for a spiral passing through three specified points in one turn and from the absence of an assumption that the order in which the spiral passes the points is known to us in advance

When  $R'_0 \rightarrow \pm\infty$ , the function  $f(R'_0) \rightarrow 0$ , as can be seen from the following asymptotic expressions. When  $R'_0 \rightarrow +\infty$  for any configuration of points and when  $R'_0 \rightarrow -\infty$  for  $\Lambda_1 \leq 0$ ,  $\Lambda_2 < 0$ , and  $\Lambda_3 < 0$ ,

$$f(R'_0) = [(Y_3 - Y_2)X_1 + (Y_1 - Y_3)X_2 + (Y_2 - Y_1)X_3]/R_0'^2 + o(1/R_0'^2); \quad (14)$$

when  $R'_0 \rightarrow -\infty$ ,

$$\text{for } \Lambda_1 \leq 0, \Lambda_2 > 0, \Lambda_3 > 0 \quad f(R'_0) = 2\pi(X_2 - X_3)/R'_0 + o(1/R'_0); \quad (15)$$

$$\text{for } \Lambda_1 \leq 0, \Lambda_2 < 0, \Lambda_3 > 0 \quad f(R'_0) = 2\pi(X_2 - X_1)/R'_0 + o(1/R'_0). \quad (16)$$

Here, the numbering of points (generally not the initial one) is set according to the above rule, the position of the spiral pole in the region of negative  $X$  corresponds to a negative  $R_0$ . The sign of the functions equivalent to  $f(R'_0)$  in all cases (14)–(16) depends only on the coordinates of points  $M_j$ , but not on  $R'_0$ . This means that when  $R'_0 \rightarrow \pm\infty$ , the function  $f(R'_0)$  asymptotically approaches the horizontal axis without crossing it. Consequently, the roots of Eq. (10) exist only in a limited interval of  $R'_0$  (including the initial  $R_0$ ). This is confirmed by direct calculations of  $f(R'_0)$  (see the examples in 1 and 2). The function  $f(R'_0)$  at an argument close to  $X_1$  or  $X_2$  or  $X_3$  can undergo sharp oscillations and suffers discontinuities due to the change of the order in which the points are numbered at configuration degeneracies ( $\Lambda_j = \Lambda_m, j \neq m$ ) (see the insets in Fig. 2).

Our calculations show that  $f(R'_0) = 0$  is generally reached at one, two, or three points. One root is fixed ( $R'_0 = R_0 = 8.0$  kpc), the *additional* roots change their positions depending on the Galactocentric longitudes  $\Lambda_1$ ,  $\Lambda_2$ , and  $\Lambda_3$ .

If the spiral segment bounded by points  $M_1$  and  $M_3$  *crosses the  $X$  axis* (the Galactic center–anticenter line), then the number of roots of the equation  $f(R'_0) = 0$  depends on the arrangement of points on the initial spiral. Figures 1a–1c present examples of the functions  $f(R'_0)$  for those configurations of points at which the number of roots is one, two, or three. In special cases, the number of roots is sensitive even to slight changes in the longitude of one point, for example, to changes in  $\Lambda_3$  if this is the only positive longitude,  $\Lambda_3$  is small, and the interval between  $\Lambda_j$  is large (Fig. 1d); note that for the family  $f(R'_0)$  in Fig. 1d in the interval  $\Lambda_3 \in (14^\circ, 15^\circ)$  there exists a value at which the number of roots is two.

In the case where the segment is located *on one side of the  $X$  axis*, including the cases where one of its (extreme) points  $M_1$  and  $M_3$  is exactly on the  $X$  axis, there always exist two roots one of which coincides with the initial  $R_0$  (Fig. 2).

A spiral passing through all three initial points corresponds to each root of the function  $f(R'_0)$  and the two remaining parameters calculated for it from Eqs. (11) and (12) (see the examples in Fig. 3), i.e., the number of such spirals is equal to the number of roots. Thus, generally, the logarithmic spiral passing through three points in one turn cannot be unambiguously determined from them even if the direction to the spiral pole is known.

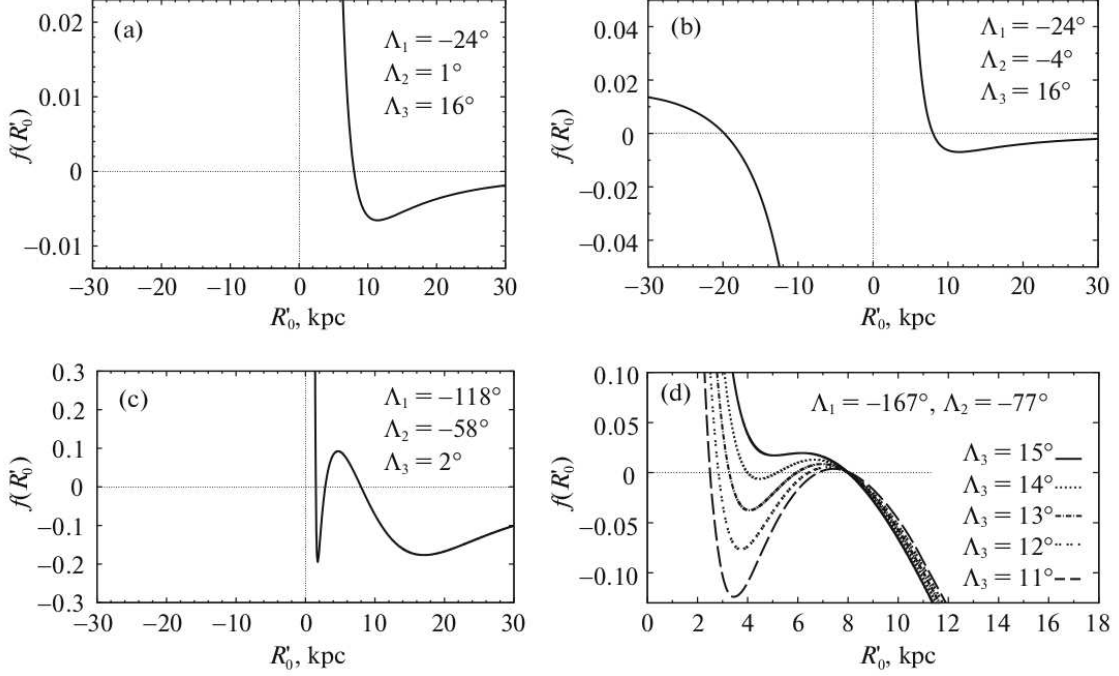


**Fig. 1.** Graphs of the functions  $f(R'_0)$  for segments crossing the direction to the spiral pole. (a)–(c) Examples of  $f(R'_0)$  with a different number of roots. (d) An example of the dependence of the number of roots  $f(R'_0)$  on longitude  $\Lambda_3$ . The initial numbering of points is indicated.

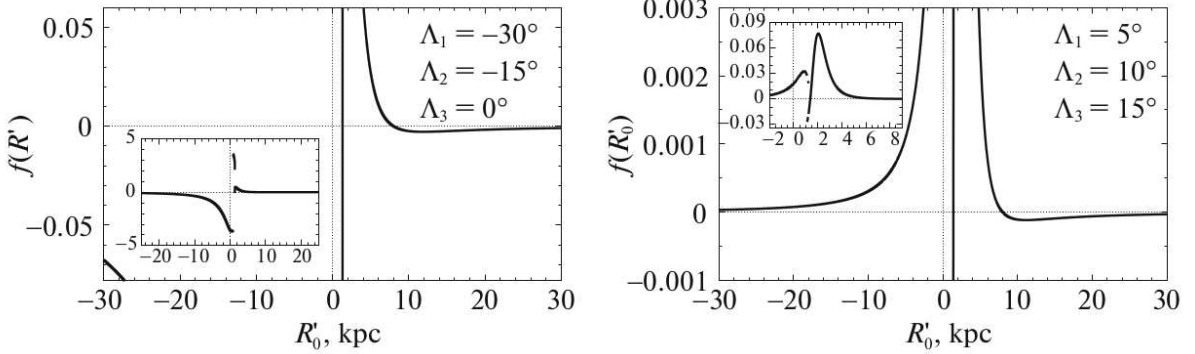


**Fig. 2.** Graphs of the functions  $f(R'_0)$  for segments located on one side of the direction to the spiral pole. The insets show graphs of the same functions for larger intervals of values. In the neighborhoods of the roots  $R'_0 \approx 1.30$  kpc on the left panel and  $R'_0 \approx 1.39$  kpc on the right panel  $f(R'_0)$  has a large, but finite, positive derivative. The initial numbering of points is indicated.

We will consider the revealed trends in more detail using the case (important for some applications) of initial points  $M_j$  equidistant in longitude  $\Lambda$  as an example. Denote the parameter  $R_0$  of the initial spiral by  $R_{0,1}$  and the additional roots of (10), if they exist, by  $R_{0,2}$  and  $R_{0,3}$ . Let us investigate the dependence of the presence/absence of additional roots and quantities  $R_{0,2}$  and  $R_{0,3}$  on the positions of the triplets of initial points  $\{M_{1,n}, M_{2,n}, M_{3,n}\}_{n=1}^N$  lying on the initial spiral. We will specify the initial longitudes of



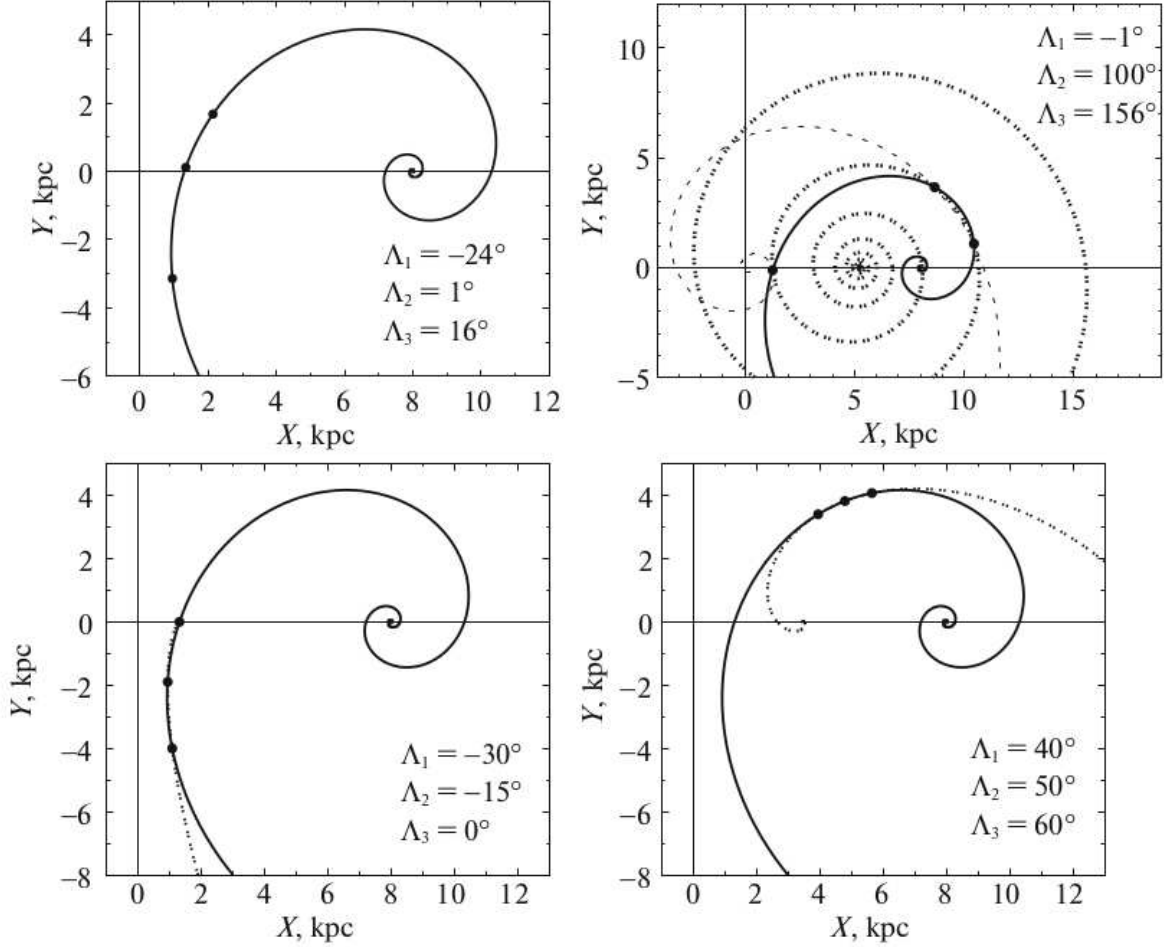


**Fig. 3.** Examples of the configurations of initial points at which the segment formed by them crosses the direction to the spiral pole (upper panels) or is located on one side of this direction (lower panels). The solid line indicates the initial spiral. On the lower left panel the pole of the additional spiral is near point  $M_3$ . The numbering of points is initial.

these points as follows:

$$\begin{aligned}
 \Lambda_{2,n} - \Lambda_{1,n} &\equiv \Delta\Lambda \equiv \Lambda_{3,n} - \Lambda_{2,n}, \\
 \Lambda_{1,n+1} - \Lambda_{1,n} &= 1^\circ, \\
 \Lambda_{1,1} &= -180^\circ, \quad \Lambda_{3,N} = 180^\circ - 1^\circ = 179^\circ.
 \end{aligned}
 \tag{17}$$

Thus, the (almost complete) spiral turn was covered by the triplets of points with a  $1^\circ$  step. A set of solutions was determined for each triplet.

In Fig. 4a the roots of  $f(R'_0)$  are plotted against the longitude of point  $M_2$  at some values of  $\Delta\Lambda$  for the model representing the Sagittarius arm. The number of roots for the triplet of points with specified  $\Delta\Lambda$  and  $\Lambda_2$  is equal to the number of intersections of the straight line  $\Lambda_2 = \text{const}$  with the branches of solutions shown in the figure (including the branch  $R_{0,1} = 8$  kpc) for this  $\Delta\Lambda$ . A generalization of the results obtained is presented in Fig. 5a for the  $(\Lambda_2, \Delta\Lambda)$  configuration plane on which the region of possible configurations (RPC) in our statement of the problem is bounded by the isosceles triangle with vertices  $(\Lambda_2, \Delta\Lambda) = (-\pi, 0), (\pi, 0), (0, \pi)$ . The RPC does not form a closed set, because the right

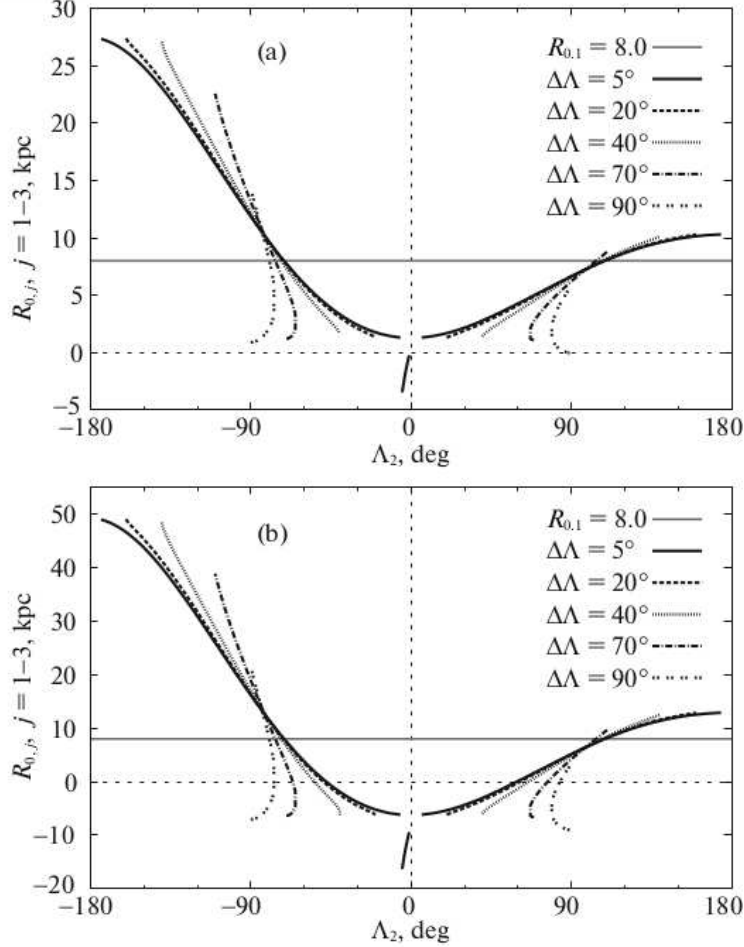


**Fig. 4.** Branches of solutions for the equation  $f(R'_0) = 0$  as functions of the longitude of the central point in the triplet at different  $\Delta\Lambda$  for the spirals representing the Sagittarius (a) and Perseus (b) arms.

side of the triangle (by definition,  $\Lambda_3 < \pi$ ) and its base (by definition,  $\Delta\Lambda > 0$ ) do not belong to it. Analysis of the graphs for the branches of solutions (Fig. 4a) and the results of scanning according to the rule (17) show that the RPC is divided into six two-dimensional regions all points of each of which have the same number of roots (Fig. 5a).

The region of a unique root ( $R_{0,1} = 8$  kpc) occupying slightly less than half of the RPC area is largest. The overwhelming majority of triplets whose segments cross the  $X$  axis, with all triplets with  $\Lambda_2 = 0$  being among them, belong to it. The properties of the region of a unique root turn out to be the same for the models of other Galactic arms as well, i.e., the three-point configurations with a unique solution of Eq. (10) correspond to the arm segments in the solar sector of the Galaxy. Such segments are usually revealed by tracers with non-kinematic (i.e., more reliable) distances (see, e.g., Popova and Loktin, 2005; Nikiforov and Kazakevich 2009; Dambis et al. 2015).

Two roots exist in the two large regions that are bounded by the triangles with vertices  $(\Lambda_2, \Delta\Lambda) = (-\pi, 0), (0, 0), (-\frac{\pi}{2}, \frac{\pi}{2})$  and  $(0, 0), (0, \pi), (\frac{\pi}{2}, \frac{\pi}{2})$  and that occupy together exactly  $\frac{1}{2}$  of the RPC area (Fig. 5a). However, the segments lying on one side of the  $X$

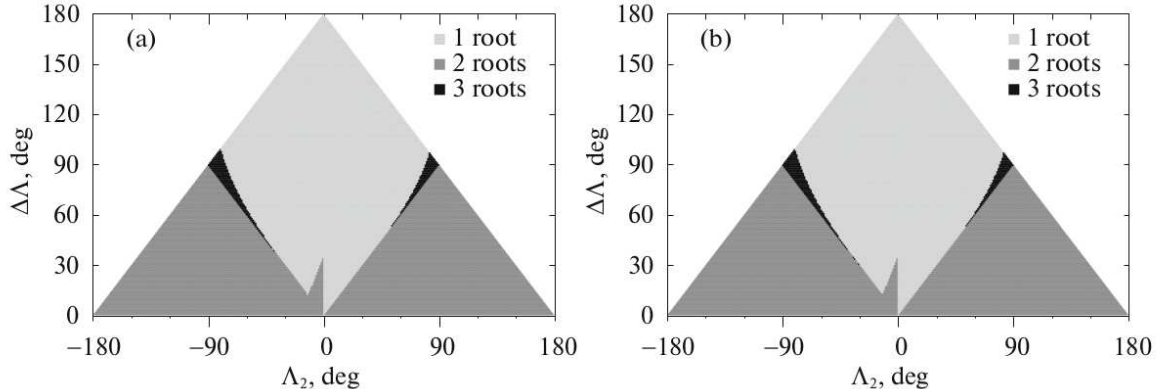


**Fig. 5.** Dependence of the number of roots of Eq. (10) on the longitude of the central point  $\Lambda_2$  and the distance between the adjacent points  $\Delta\Lambda$  for the spirals representing the Sagittarius (a) and Perseus (b) arms.

axis, including the cases where the extreme point ( $\Lambda_1 = 0$  or  $\Lambda_3 = 0$ ) touches this axis, correspond to them, and such configurations are not typical of tracers with non-kinematic distances.

Between these regions of two roots and the region of a unique root there are small (in area) two-dimensional regions of three roots bounded, respectively, by the line  $\Lambda_2 = -\Delta\Lambda$  and the line  $\Lambda_2 = +\Delta\Lambda$  (Fig. 5a). The first region is revealed at  $39^\circ \leq \Delta\Lambda \leq 99^\circ$  for triplets with  $\Lambda_{1,n} < -\Delta\Lambda < \Lambda_{2,n} < 0 < \Lambda_{3,n}$ . The second region is revealed at  $54^\circ \leq \Delta\Lambda \leq 97^\circ$  for triplets with  $\Lambda_{1,n} < 0 < \Lambda_{2,n} < \Delta\Lambda < \Lambda_{3,n}$ .

A small region of two roots that has a triangular shape and is bounded by the lines  $\Lambda_2 = 0$  and  $\Lambda_2 = -\Delta\Lambda$ , but does not include them, is also revealed at  $\Delta\Lambda \leq 34^\circ$  (Fig. 5a). The region corresponds to short segments crossing the  $X$  axis with  $\Lambda_{1,n} < -\Delta\Lambda < \Lambda_{2,n} < 0 < \Lambda_{3,n}$ . However, even when  $\Lambda_2 \rightarrow -0$  for fixed  $\Delta\Lambda$ , the additional root  $R_{0,2}$  is much smaller than the initial  $R_0 = 8$  kpc, while it becomes even smaller as  $\Lambda_2$  decreases; the dependence  $R_{0,2}(\Lambda_2)$  suffers a discontinuity at  $\Lambda_2 = -\Delta\Lambda$ , and the solution  $R_{0,2}$  abruptly passes to another branch with larger values (see the graph for  $\Delta\Lambda = 5^\circ$  in Fig. 4a). As  $\Delta\Lambda$  increases, the branch  $R_{0,2}(\Lambda_2)$  at  $-\Delta\Lambda < \Lambda_2 < 0$  goes abruptly into the negative region. Therefore, this branch fell into the interval of  $R_{0,j}$  shown in Fig. 4a only for  $\Delta\Lambda = 5^\circ$ . As the lower limit of the search for roots decreases, the height of the region of two roots under consideration increases (but very slowly) due to the upward shift of its upper inclined boundary (in Fig. 5a this region is given for  $R'_0 \geq -5000$  kpc). Obviously, the presence of such a branch of solutions deviating strongly from the initial value of  $R_{0,1}$  does not produce any ambiguity in choosing the root.

The same is also true for most of the length of other branches of additional roots (Fig. 4a), where the solutions are distinguishable from the initial spiral in pitch angle as well. The cases where the middle point of the segment is near the traverse directions,  $\Lambda_{2,n}$  from  $-80^\circ$  to  $-70^\circ$  and from  $+100^\circ$  to  $+115^\circ$  (the intervals of intersections of the line  $R_{0,1} = 8$  kpc by the branches of additional roots in Fig. 4a), constitute an exception. Such situations are quite possible when analyzing the spiral arm segments using masers

the data on which cover predominantly quadrants I and II (e.g., Reid et al. 2014; see also Section 3 in this paper). This means that some algorithm for choosing between the roots  $R_{0,j}$  is generally needed.

Finally, there exist two degenerate one-dimensional regions (i.e., lines) of two roots to which the merging/bifurcation points of the branches of two additional roots, where these branches have infinite derivatives, correspond in Fig. 4a. In Fig. 5a these lines form the boundaries between the region of one root and the regions of three roots. Having zero area, the lines of two roots for an arbitrary scanning of type (17) are not revealed and, therefore, are not displayed in Fig. 5a.

The same study was performed for the model spiral representing the Perseus arm with parameters  $R_0 = 8.0$  kpc,  $i = -18^\circ$ , and  $\lambda_0 = 97^\circ$  (Nikiforov and Shekhovtsova 2001). The results obtained (Figs. 4b and 5b) show that the basic properties of the solutions of Eq. (10) remain as before when passing from the inner spiral arm to the outer one. The differences concern only some details. For the Perseus arm the lower parts of all branches of additional roots lie in the region  $R_0 < 0$  kpc (because many of the triplets near the outer arm have negative coordinates  $X_j$ ), the scatter of values of  $R_{0,2}$  and  $R_{0,3}$  turns out to be larger, and the left region of three roots is revealed at  $\Delta\Lambda \geq 31^\circ$  (for the Sagittarius arm at  $\Delta\Lambda \geq 39^\circ$ ). The remaining parameters of the small regions of two and three roots are the same as those for the Sagittarius arm to within  $1^\circ$ .

On the whole, the changes of the results are insignificant when varying the pitch angles of the initial spirals as well. The quantity  $i$  affects only some characteristics of the small regions: the region of two roots adjacent to the line  $\Lambda_2 = 0$  is reduced with decreasing  $|i|$  (at  $i = -10^\circ$  for both arms  $(\Delta\Lambda)_{\max} = 17^\circ$ ); the lower (in  $\Delta\Lambda$ ) boundary of the left region of three roots slightly varies.

### *2.3. On the Possibility of Determining the Parameters of a Logarithmic Spiral from Four Points*

Since the three-point method generally yields an ambiguous result, let us consider the possibility of reconstructing the parameters of a spiral from four points  $M_j$ ,  $j = 1, 2, 3, 4$ , located on one its turn. From the quadruplet of points we will single out two arbitrary triplets  $M_1, M_2, M_3$  and  $M_1, M_3, M_4$ , write equations of the form (10) for them, and pose the problem to find the same solution for both triplets. This leads to the equation for  $R_0$

$$f_4(R'_0) \equiv |f_{123}| + |f_{134}| = 0, \quad (18)$$

where

$$f_{123}(R'_0) = (\ln R_1 - \ln R_2)(\lambda_2 - \lambda_3) + (\ln R_3 - \ln R_2)(\lambda_1 - \lambda_2), \quad (19)$$

$$f_{134}(R'_0) = (\ln R_1 - \ln R_3)(\lambda_3 - \lambda_4) + (\ln R_4 - \ln R_3)(\lambda_1 - \lambda_3). \quad (20)$$

The moduli in (18) are needed to avoid the extraneous roots at such  $R_0$  that  $f_{123} = -f_{134} \neq 0$  to which the spirals passing through four (and even three) points do not correspond.

**Table 1.** Data on the spiral segments identified by Reid et al. (2014) based on masers.  $l_{\min}$ ,  $l_{\max}$ , and  $\Delta l$  are the boundaries and the extent in Galactic longitude

Segment	Number of masers	$l_{\min}$	$l_{\max}$	$\Delta l$
Scutum arm	17	$6^\circ$	$32^\circ$	$26^\circ$
Sagittarius arm	18	$-9^\circ$	$52^\circ$	$61^\circ$
Local arm	25	$60^\circ$	$239^\circ$	$179^\circ$
Perseus arm	24	$43^\circ$	$241^\circ$	$198^\circ$
Outer arm	6	$75^\circ$	$196^\circ$	$121^\circ$

A check showed that Eq. (18) actually has a unique root at the point where the positive-definite function  $f_4(R'_0)$  touches the horizontal axis. However, even at a small variation in the position of at least one point  $M_j$  Eq. (18) generally becomes unsolvable, because arbitrary four points do not lie on one spiral turn. This makes the potential four-point method inapplicable to pseudo-random or real data. This property is retained as the number of initial points increases further.

On the other hand, an arbitrary triplet of points lies on one turn of at least one spiral, and, hence, at least one solution will always exist when varying the positions of the points. Therefore, the three-point method can be applied to real data and in numerical experiments provided that a criterion for choosing between the roots is introduced. Below we will use the three-point method.

### 3. APPLYING THE THREE-POINT METHOD OF DETERMINING THE SPIRAL PARAMETERS TO THE DATA ON MASERS

The formal apparatus to determine a spiral from initial points is needed as a simple tool for studying the possibilities of estimating  $R_0$  from the geometry of spiral arm segments as a function of problem parameters by the method of numerical simulations. Such a study will be performed in the next paper.

However, the three-point method also allows the new approach to be immediately tested on real data. To solve this problem, we chose maser sources with trigonometric parallaxes, because they undoubtedly meet all three requirements for performing the spatial modeling of individual arm segments formulated in the Introduction and have absolute (needing no calibration) heliocentric distance measurements. The data were taken from the catalogue of H<sub>2</sub>O and CH<sub>3</sub>OH masers in high-mass star-forming regions (Reid et al. 2014). The catalogue contains the characteristics of 103 masers from the BeSSeL, VERA, VLBI, and EVN surveys; the mean parallax accuracy is 20  $\mu$ as. Based on these data, Reid et al. (2014) identified five spiral segments, assigning the vast majority of masers to a particular segment by associating the positions of masers with CO and HI emission features on the  $l - V_{\text{LSR}}$  diagram, where  $V_{\text{LSR}}$  is the line-of-sight velocity relative to the local standard of rest. In this paper we adopt the distribution of masers over the segments proposed by Reid et al. (2014) (for the observational characteristics of the segments, see Table 1).

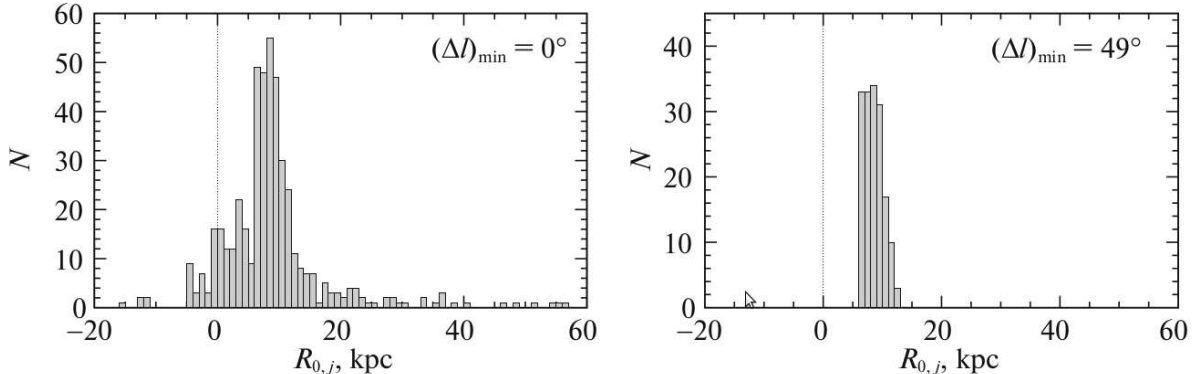


**Fig. 6.**  $R_{0,j}$  distribution function for the Perseus arm at  $(\Delta l)_{\min} = 0^\circ$  (the complete set of all possible triplets of masers) and at optimal  $(\Delta l)_{\min} = 49^\circ$ .

### 3.1. The Algorithm

Each sample of masers assigned to one of the segments was analyzed separately using an algorithm based on the three-point method. The distance errors for the maser sources were disregarded at this stage (checking whether the approach is operable). From the masers of each sample only those sets of three objects  $M_{1,j}$ ,  $M_{2,j}$ , and  $M_{3,j}$  were selected for which the angular distance between the adjacent objects  $l(M_{m+1,j}) - l(M_{m,j})$ ,  $m = 1, 2$  was no less than some adopted value  $(\Delta l)_{\min}$  (here,  $j$  is the set number);  $(\Delta l)_{\min}$  was reoptimized for each sample. For each of the selected triplets of objects we calculated the values of  $R_0$  as the roots of Eq. (10) and the parameters  $k$  and  $\lambda_0$  corresponding to them from Eqs. (11) and (12).  $R_0$  was sought in the segment  $[-60.0, 60.0]$  kpc. We considered two techniques for processing the cases of a nonunique solution for  $R_0$ : (1) eliminating the triplets with a nonunique solution and (2) choosing such a root from  $R_{0,1,j}$ ,  $R_{0,2,j}$ , and, possibly,  $R_{0,3,j}$  that leads to the smallest scatter of sample masers relative to the spiral determined by them. The first technique is simple and more reliable, but it is applicable only at a significant fraction of triplets with a unique solution in the total sample. Since the spiral arms turn out to be the trailing ones from these data (Reid et al. 2014), the triplets corresponding to the leading spirals (with  $k_j > 0$ ) were excluded from consideration in both techniques.

At fixed  $(\Delta l)_{\min}$  the point estimates of the parameters  $R_0$ ,  $k$ , and  $\lambda_0$  for the segment under consideration were defined as the medians (Me) of the sets  $\{R_{0,j}\}$ ,  $\{k_j\}$ , and  $\{\lambda_{0,j}\}$  obtained from all of the triplets  $\{M_{1,j}, M_{2,j}, M_{3,j}\}$  left after the eliminations by one of the above techniques; here,  $j = 1, \dots, N_{\text{sol}}$ , where  $N_{\text{sol}}$  is the number of solutions involved in the processing. As an optimal  $(\Delta l)_{\min}^0$  we then chose  $(\Delta l)_{\min}$  for which the variance of the mean  $\langle R_0 \rangle$  was smallest. As the final result for the segment sample we took the estimates of Me  $R_0$ , Me  $k$ , and Me  $\lambda_0$  found for  $(\Delta l)_{\min}^0$ . We calculated the boundaries of min the  $1\sigma$  confidence intervals for these estimates based on order statistics (see, e.g., Kobzar’ 2006).

For the *model spiral* (with the parameters Me  $R_0$ , Me  $k$ , and Me  $\lambda_0$  obtained at  $(\Delta l)_{\min} = (\Delta l)_{\min}^0$ ) we determined the  $1\sigma$  confidence region (see Appendix A1). Below we

give this region for the Perseus arm; for other segments the boundaries of the confidence regions, being less regular in pattern, are not informative. For all segments we also made an attempt to estimate the natural root-mean-square (rms) scatter  $(\sigma_w)_0$  of masers across the spiral arm (see Appendix A2).

In this way we processed the samples of masers for all five Galactic spiral arm segments identified by Reid et al. (2014).

### 3.2. Results for the Individual Spiral Segments

The most reliable estimates of the model parameters were obtained for the sample of 24 masers assigned to the Perseus arm. For this segment the triplets of masers through which more than one spiral passed were excluded from consideration.  $(\Delta l)_{\min}$  was varied from  $0^\circ$  (the complete set of triplets was used) to  $70^\circ$ .

Comparison of the  $R_{0,j}$  distributions at various values of  $(\Delta l)_{\min}$  shows that as  $(\Delta l)_{\min}$  increases, the number of negative values of  $R_{0,j}$  decreases, as does the variance of the distribution. For triplets with  $(\Delta l)_{\min} \geq 49^\circ$  the values of  $R_{0,j}$  lie in the positive region and are grouped in the segment  $[6, 13]$  kpc (Fig. 6).

The results of our analysis of the positions of Perseus arm masers for various values of  $(\Delta l)_{\min}$  are summarized in Table 2. These results show that as  $(\Delta l)_{\min}$  increases, the error of the mean  $\sigma_{\langle R_0 \rangle}$  and the confidence interval for the median of  $R_{0,j}$  initially decrease because of the truncation of the  $R_{0,j}$  distribution wings (Fig. 6) and, once the variance of this distribution has achieved stabilization (see the row of standard deviations  $\sigma_{R_0}$  in Table 2), grow due to the reduction in the sample size (the number of solutions  $N_{\text{sol}}$ ). This makes it possible to choose an optimal longitude constraint  $(\Delta l)_{\min}^0$  from the minimum of the formal error of the mean  $\sigma_{\langle R_0 \rangle}$  (a more stable dispersion characteristic than the length of the confidence interval for the median). For the Perseus arm we found  $(\Delta l)_{\min}^0 = 49^\circ$ . The model spiral corresponding to this constraint in comparison with the positions of the masers is presented in Fig. 7.

The parameters of other spiral segments were determined in a similar way. All masers of the Scutum arm and almost all masers of the Sagittarius arm are on one side of the  $X$  axis (Figs. 8b and 9b), and, consequently, all triplets of masers in the first case and almost all of them in the second one give two solutions for each  $R_0$  (see Subsection 2.2). Excluding the triplets with a nonunique solution is then inapplicable for these segments. Therefore, we used an alternative processing: for each such triplet we chose the root for which the sum of the squares of the distances from the spiral corresponding to it to the remaining masers of the segment under consideration was smaller. The Outer arm was processed in the same way, because it is represented by a small number of objects ( $N = 6$ ). The  $R_{0,j}$  distributions and the model spirals constructed for these three segments at  $(\Delta l)_{\min}^0 = 0^\circ$  in comparison with the positions of the masers are shown in Figs. 8–10.

For the Local arm we considered both techniques of processing the triplets with a nonunique solution for  $R_0$ . A visualization of the results obtained is presented in Figs. 11

**Table 2.** Results of applying the three-point method to the Perseus arm masers

$(\Delta l)_{\min}$	0°	5°	15°	30°	40°	49°	50°	60°	70°
$N_{\text{sol}}$	462	445	335	237	213	161	159	104	34
$\langle R_0 \rangle$	8.79	9.26	9.48	8.47	7.75	8.55	8.55	8.54	9.07
$\sigma_{R_0}$	8.74	8.55	7.04	5.28	3.52	1.51	1.52	1.51	1.48
$\sigma_{\langle R_0 \rangle}$	0.41	0.41	0.38	0.34	0.24	0.119	0.121	0.15	0.25
<b>Me <math>R_0</math></b>	<b>8.11</b>	<b>8.25</b>	<b>8.46</b>	<b>8.23</b>	<b>8.20</b>	<b>8.43</b>	<b>8.41</b>	<b>8.42</b>	<b>8.92</b>
$\sigma^+(\text{Me } R_0)$	+0.22	+0.21	+0.29	+0.20	+0.17	+0.19	+0.21	+0.35	+0.69
$\sigma^-(\text{Me } R_0)$	-0.22	-0.24	-0.23	-0.26	-0.30	-0.20	-0.18	-0.20	-0.55
<b>Me <math>i</math></b>	<b>-9°69</b>	<b>-9°85</b>	<b>-9°83</b>	<b>-9°76</b>	<b>-9°75</b>	<b>-10°61</b>	<b>-10°43</b>	<b>-10°61</b>	<b>-12°1</b>
$\sigma^+(\text{Me } i)$	+0°35	+0°27	+0°47	+0°91	+1°05	+0°75	+0°57	+0°64	+1°3
$\sigma^-(\text{Me } i)$	-0°23	-0°19	-0°22	-0°64	-0°65	-0°64	-0°95	-1°54	-3°7
<b>Me <math>\lambda_0</math></b>	<b>78°2</b>	<b>78°7</b>	<b>73°0</b>	<b>73°0</b>	<b>78°4</b>	<b>60°7</b>	<b>61°4</b>	<b>61°1</b>	<b>52°1</b>
$\sigma^+(\text{Me } \lambda_0)$	+7°6	+8°5	+6°1	+6°8	+10°5	+10°0	+9°5	+9°8	+10°6
$\sigma^-(\text{Me } \lambda_0)$	-7°3	-5°7	-8°6	-9°8	-13°3	-2°8	-3°3	-2°9	-10°4
$(\sigma_w)_\varpi$	0.23	0.23	0.23	0.24	0.23	0.25	0.25	0.25	0.24
$(\sigma_w)_{\text{obs}}$	0.44	0.48	0.44	0.43	0.45	0.46	0.46	0.45	0.44
$(\sigma_w)_0$	0.37	0.42	0.37	0.35	0.39	0.38	0.39	0.38	0.37

$\langle R_0 \rangle$  and  $\sigma_{\langle R_0 \rangle}$  are the arithmetic mean of  $N_{\text{sol}}$  values of  $R_{0,j}$  and its error;  $\sigma_{R_0}$  is the standard deviation of the  $R_{0,j}$  distribution;  $\sigma^+$  and  $\sigma^-$  are the statistical uncertainties of the median for the 1 $\sigma$  confidence level toward larger and smaller values, respectively;  $(\sigma_w)_\varpi$  is the contribution to the scatter of masers across the segment from the parallax uncertainty;  $(\sigma_w)_{\text{obs}}$  and  $(\sigma_w)_0$  are, respectively, the observed and natural rms scatters across the segment.  $R_0$ ,  $(\sigma_w)_\varpi$ ,  $(\sigma_w)_{\text{obs}}$ , and  $(\sigma_w)_0$  are given in kiloparsecs.

and 12. We took the results obtained by excluding the triplets with a nonunique solution as the final ones for this segment, because the model spiral describes better the positions of the segment masers in this case (cf. Figs. 11b, 12b).

A summary of the main results for the individual Galactic spiral arm segments is given in Table 3. The absence of  $(\sigma_w)_0$  for the Outer and Scutum arms in the last column of the table corresponds to a negative estimate of the natural variance across the arm  $(\sigma_w)_0^2$ . This means that the observed scatter of masers relative to these segments is entirely (and even excessively) explained by the catalogue uncertainties of the trigonometric parallaxes in Reid et al. (2014) (see Section 5).

Since the results for the individual segments were obtained from small samples of objects, it is important to estimate the biases of  $R_0$  and other parameters found by the three-point method due to the sample finiteness. This was done using the jackknife technique (see Appendix A3) that also allows the variances of parameters to be estimated. The



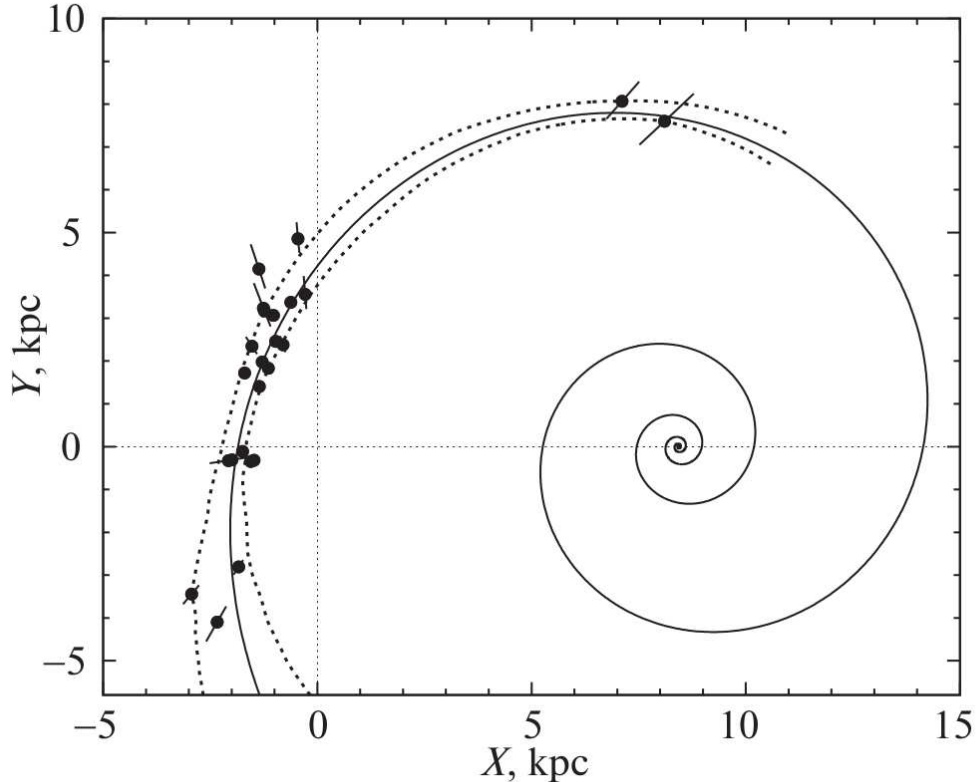


**Fig. 7.** The distribution of Perseus arm masers in projection onto the Galactic plane and the model spiral constructed for them by the three-point method at  $(\Delta l)_{\min}^0 = 49^\circ$ . The error bars reflect the parallax uncertainty. The dotted lines mark the boundaries of the  $1\sigma$  confidence region for the model spiral.

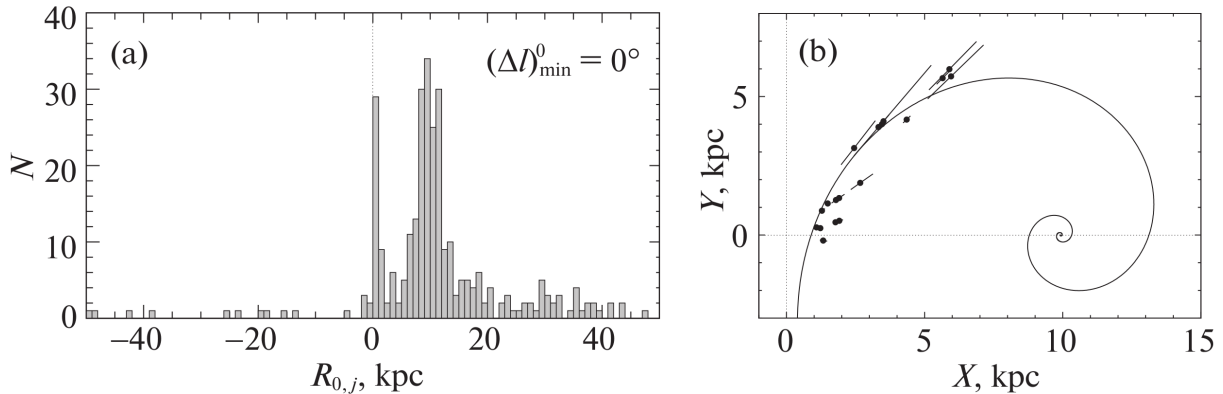


**Fig. 8.** Visualization of the results of applying the three-point method to the Sagittarius arm at  $(\Delta l)_{\min}^0 = 0^\circ$ . (a) The  $R_{0,j}$  distribution. (b) The model spiral in comparison with the positions of the masers assigned to this arm in projection onto the Galactic plane (the error bars reflect the parallax uncertainty).

corrected results are presented in Table 4. Comparison with Table 3 shows that the jack-knife uncertainties of the parameters turned out to be appreciably larger than the formal uncertainties of the median estimates in the overwhelming majority of cases. Obviously,

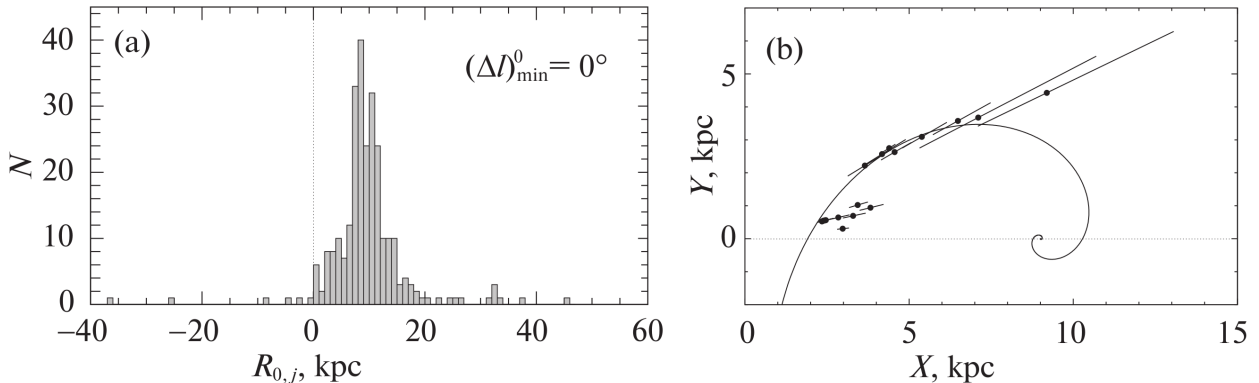


**Fig. 9.** Same as Fig. 8 for the Scutum arm;  $(\Delta l)_{\min}^0 = 0^\circ$ .

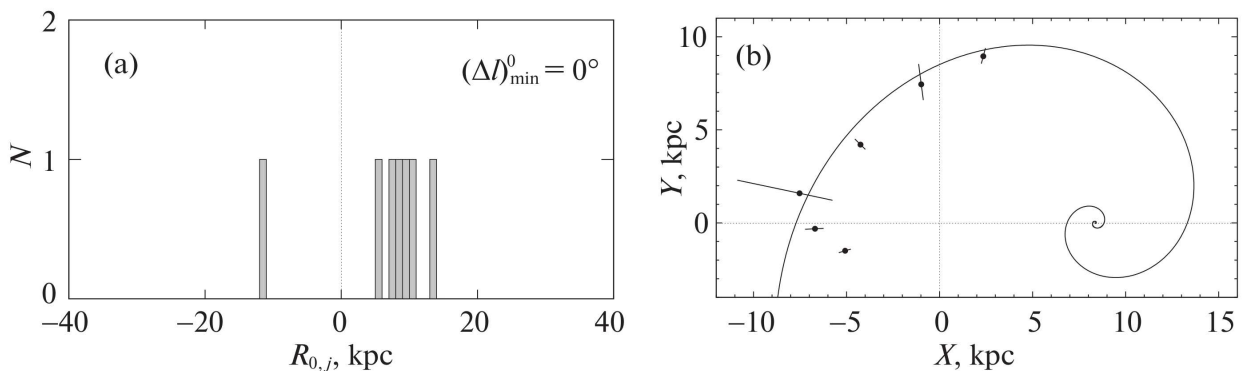


**Fig. 10.** Same as Fig. 8 for the Outer arm;  $(\Delta l)_{\min}^0 = 0^\circ$ .

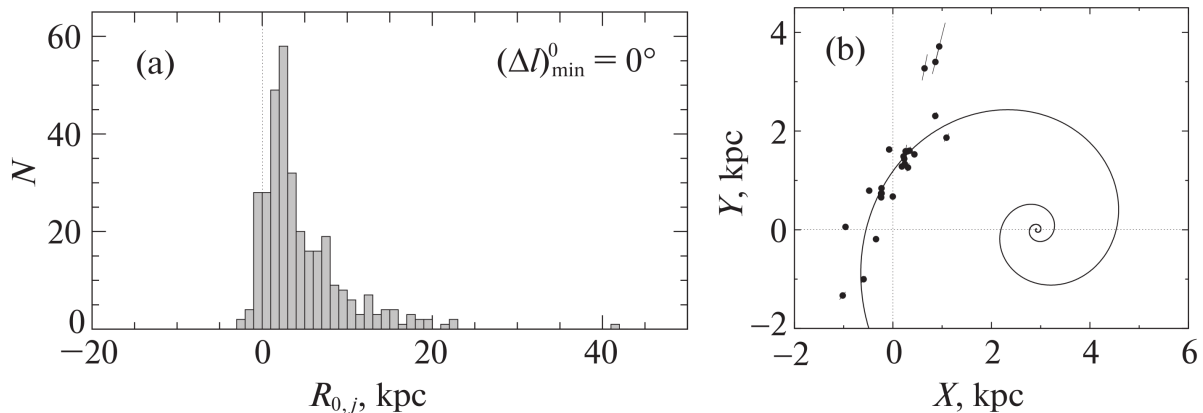


**Fig. 11.** Same as Fig. 8 for the Local arm. The triplets with multiple roots of the equation for  $R_0$  were excluded from consideration;  $(\Delta l)_{\min}^0 = 0^\circ$ .

this is explained by the fact that each sample object, as a rule, enters into different triplets, and this makes the results for individual triplets not quite independent. The latter is naturally taken into account when using the jackknife technique. Our numerical experiments (see Section 4) confirm that the jackknife estimates of the variances are more adequate. For completeness, we provide both error estimates. For practical purposes, we will choose the larger of them.

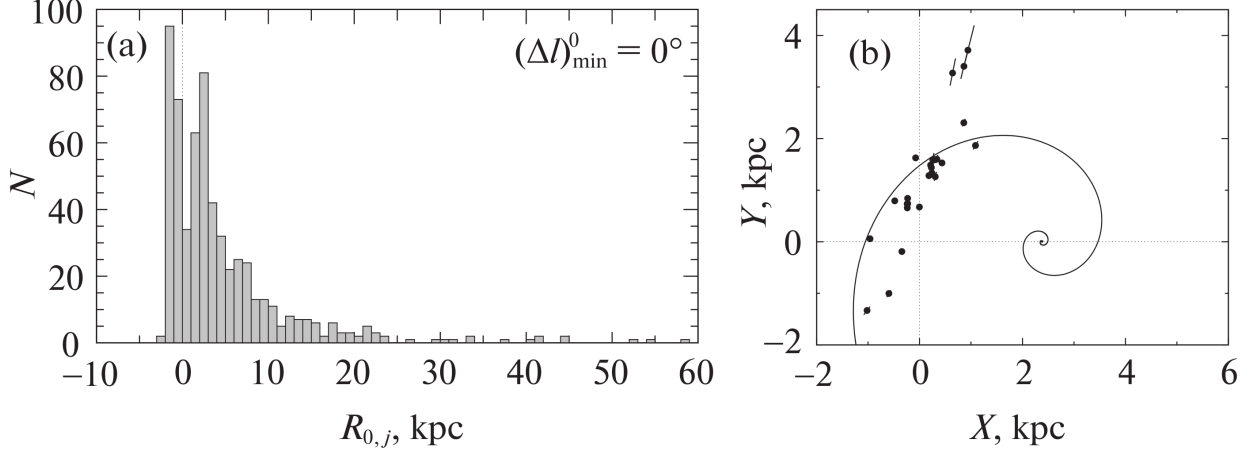


**Fig. 12.** Same as Fig. 11 when choosing the solution with the smallest scatter of masers relative to the model spiral from the multiple roots;  $(\Delta l)_{\min}^0 = 0^\circ$ .

**Table 3.** Results of applying the three-point method to five spiral arm segments for optimal longitude constraints  $(\Delta l)_{\min}^0$

Arm	$N_{\text{sol}}$	$(\Delta l)_{\min}^0$	Me $R_0$ , kpc	Me $i$	Me $\lambda_0$	$(\sigma_w)_0$ , kpc
Sct	267	$0^\circ$	$9.01^{+0.30}_{-0.15}$	$-28^\circ 64^{+1.40}_{-1.59}$	$-25^\circ 0^{+3.5}_{-4.5}$	0.34
Sgr	306	$0^\circ$	$9.92^{+0.36}_{-0.34}$	$-18^\circ 29^{+0.99}_{-1.13}$	$-16^\circ 4^{+2.4}_{-3.9}$	
Loc	328	$0^\circ$	$2.93^{+0.35}_{-0.19}$	$-13^\circ 85^{+0.39}_{-0.37}$	$+39^\circ 7^{+6.7}_{-4.9}$	
Per	161	$49^\circ$	$8.43^{+0.19}_{-0.20}$	$-10^\circ 61^{+0.75}_{-0.64}$	$+60^\circ 7^{+10.0}_{-2.8}$	
Out	7	$0^\circ$	$8.4^{+5.3}_{-19.6}$	$-20^\circ 6^{+16.9}_{-58^\circ}$	$+100^\circ ^{+521^\circ}_{-56^\circ}$	

**Table 4.** Results of correcting the estimates of the spiral segment parameters by the jackknife technique

Arm	$R_{0,\text{corr}} \pm \sigma_{R_{0,J}}$ , kpc	$\Delta R_0$ , kpc	$i_{\text{corr}} \pm \sigma_{i,J}$	$\Delta i$	$\lambda_{0,\text{corr}} \pm \sigma_{\lambda_{0,J}}$	$\Delta \lambda_0$
Sct	$8.62 \pm 0.81$	-0.39	$-27^\circ 2 \pm 5^\circ 4$	$+1^\circ 4$	$-21^\circ 1 \pm 12^\circ 0$	$+3^\circ 9$
Sgr	$10.62 \pm 0.69$	+0.70	$-15^\circ 5 \pm 3^\circ 6$	$+2^\circ 8$	$-12^\circ 8 \pm 8^\circ 7$	$+3^\circ 6$
Loc	$2.17 \pm 1.00$	-0.76	$-12^\circ 3 \pm 4^\circ 6$	$+1^\circ 6$	$+39^\circ 1 \pm 18^\circ 8$	$-0^\circ 6$
Per	$8.36 \pm 0.53$	-0.07	$-11^\circ 5 \pm 2^\circ 2$	$-0^\circ 9$	$+36^\circ 9 \pm 15^\circ 0$	$-23^\circ 8$
Out	$16.0 \pm 7.5$	+7.6	$+3^\circ 5 \pm 25^\circ$	$+24^\circ$	$+84^\circ \pm 40^\circ$	$-16^\circ$

$R_{0,\text{corr}}$ ,  $i_{\text{corr}}$ , and  $\lambda_{0,\text{corr}}$  are the corrected estimates of the parameters;  $\sigma_{R_{0,J}}$ ,  $\sigma_{i,J}$ , and  $\sigma_{\lambda_{0,J}}$  are the jackknife estimates of the uncertainties in the parameters;  $\Delta R_0$ ,  $\Delta i$ , and  $\Delta \lambda_0$  are the jackknife corrections to the estimates of the parameters (the differences between the corrected estimates and the median values in Table 3).

### 3.3. The Mean Estimate of $R_0$ from the Results of Applying the Three-Point Method to Masers

Table 4 shows that the results for different segments differ sharply in solution reliability. The Outer arm has the worst characteristics (the largest biases and variances of the parameters), because the sample of masers is very small in size ( $N = 6$ ). In fact, this segment creates no significant constraints on  $R_0$ , and, therefore, the result for it was not used in deducing the mean estimate of  $R_0$ . A similar decision was made with regard to the Sagittarius and Local arms. For the Sagittarius arm the  $R_{0,j}$  distribution function is definitely bimodal (Fig. 8a), suggesting that the solution is not unique; in that case, even the median estimate is unreliable (this can be seen from Fig. 8b). The model spirals for the Local arm in both versions of the three-point method agree poorly with the positions of the masers with the largest Galactocentric longitude (Figs. 11b and 12b) that, in principle, are most valuable for localizing the position of the spiral segment pole, which led to an inconsistent solution.

The results for the Perseus and Scutum arms are much more reliable: the estimates of  $R_0$  from them have the smallest biases and acceptable variances. Obviously, this is explained predominantly by the fact that the Perseus arm segment has the greatest extent (in both  $l$  and  $\Lambda$ ) and contains relatively many masers, while the Scutum arm (with a moderate number of masers) is innermost and, hence, determines better the position of the spiral pole, other things being equal (Table 1, Fig. 13).

For these reasons, we found the mean estimate  $\langle R_0 \rangle$  by this method based on the corrected values of  $R_0$  for the Perseus and Scutum arms given in Table 4 as a weighted mean with weights inversely proportional to the variances  $\sigma_{R_0,j}^2$  determined by the jackknife technique:

$$\begin{aligned} \langle R_0 \rangle &= (8.36/0.53^2 + 8.62/0.81^2) / (1/0.53^2 + 1/0.81^2) = 8.44 \text{ kpc}, \\ \sigma_{\langle R_0 \rangle} &= (1/0.53^2 + 1/0.81^2)^{-1/2} = 0.45 \text{ kpc}. \end{aligned} \tag{21}$$

At fixed  $R_0$  the three-point method becomes the two-point method of determining the segment pitch angle  $i$  and position parameter  $\lambda_0$ . In this way we estimated  $i$  and  $\lambda_0$  for all five segments at  $R_0 = 8.44$  kpc: for each segment these parameters were determined as the medians of the values obtained from all possible pairs of segment masers with the minimum distance between the pair objects  $(\Delta l)_{\min}^0$  determined by applying the three-point method to this segment. The results are presented in Table 5.

## 4. INVESTIGATION OF THE THREE-POINT ALGORITHM BY THE MONTE CARLO TECHNIQUE AND THE FINAL SOLUTION FROM MASERS

As the models of spiral arms we considered logarithmic spirals with parameters  $i$ ,  $\lambda_0$ , and  $(\sigma_w)_{\text{obs}}$  representing the Perseus and Scutum arms under the assumption of  $R_0 = 8.44$  kpc (Table 5).

**Table 5.** Results of determining the parameters  $i$  and  $\lambda_0$  and dispersion characteristics of the spiral arm segments at fixed  $R_0 = 8.44$  kpc

Arm	Me $i$	$\sigma_{i,J}$	Me $\lambda_0$	$\sigma_{\lambda_0,J}$	$(\sigma_w)_{\text{obs}}$ , kpc	$(\sigma_w)_0$ , kpc
Sct	$-21.4^{+0.6}_{-1.0}$	1:8	$-43.9^{+2.8}_{-5.7}$	10:5	$0.51 \pm 0.26$	
Sgr	$-9.9^{+1.8}_{-0.8}$	3:6	$-50.8^{+6.5}_{-16.7}$	26°	$0.37 \pm 0.08$	$0.20 \pm 0.04$
Loc	$-16.5^{+1.4}_{-2.2}$	5:1	$+9.0^{+0.3}_{-0.2}$	0:6	$0.30 \pm 0.06$	$0.29 \pm 0.04$
Per	$-10.6^{+0.6}_{-0.4}$	1:1	$+63.3^{+4.3}_{-2.1}$	9:4	$0.42 \pm 0.08$	$0.34 \pm 0.05$
Out	$-18.6^{+6.7}_{-5.6}$	0:8	$+98.0^{+26.0}_{-11.0}$	2:0	$1.19 \pm 0.49$	

$\sigma_{i,J}$  and  $\sigma_{\lambda_0,J}$  are the jackknife estimates of the uncertainties in the median values.

**Table 6.** Results of determining the parameters  $i$  and  $\lambda_0$  and dispersion characteristics of the spiral arm segments at the final  $R_0 = 8.8$  kpc

Arm	Me $i$	$\sigma_{i,J}$	Me $\lambda_0$	$\sigma_{\lambda_0,J}$	$(\sigma_w)_{\text{obs}}$ , kpc	$(\sigma_w)_0$ , kpc
Sct	$-23.7^{+1.1}_{-3.7}$	1:1	$-36.9^{+3.1}_{-6.5}$	5:7	$0.48 \pm 0.23$	
Sgr	$-9.9^{+0.5}_{-2.0}$	3:1	$-44.4^{+3.2}_{-9.7}$	22°	$0.39 \pm 0.09$	$0.29 \pm 0.08$
Loc	$-16.8^{+1.2}_{-1.3}$	5:4	$+8.5^{+0.2}_{-0.8}$	0:5	$0.30 \pm 0.06$	$0.30 \pm 0.05$
Per	$-11.8^{+0.7}_{-0.4}$	1:5	$+57.2^{+5.3}_{-1.2}$	3:8	$0.42 \pm 0.10$	$0.35 \pm 0.05$
Out	$-19.2^{+2.5}_{-2.9}$	0:9	$+91.6^{+18.1}_{-5.3}$	2:3	$1.19 \pm 0.48$	

$\sigma_{i,J}$  and  $\sigma_{\lambda_0,J}$  are the jackknife estimates of the uncertainties in the median values.

The pseudo-random catalogues of objects were generated as follows. The position of each object  $O_j$  was shifted relative to the model point  $M_j$ , which is an orthogonal projection of the nominal position (according to the initial catalogue) of the  $j$ th object onto the model spiral; the shift was done along a straight line perpendicular to the model spiral at point  $M_j$ . The distance  $\rho_j \equiv |O_j M_j|$  was varied according to a normal law with zero mean and a standard deviation  $(\sigma_w)_{\text{obs}}$ . For each of the two segments we produced  $n_{\text{MC}} = 1000$  catalogues.

For each pseudo-random catalogue the spiral segment parameters were determined by the three-point method, with the minimum distance in Galactic longitude  $(\Delta l)_{\text{min}}$  between the adjacent points ("objects") in the set of three points having been optimized in the same way as for the real data; i.e., we took  $(\Delta l)_{\text{min}}$  at which the statistical error of the mean for  $R_0$  calculated from all of the suitable triplets was minimal as the best value. The median values of the parameters with the scatter  $(\sigma_w)_{\text{obs}}$  calculated for them at optimal  $(\Delta l)_{\text{min}}$  were considered as a solution for each catalogue. Our processing of  $n_{\text{MC}}$  catalogues showed

that  $\text{Me } R_0 - R_0 = -0.66 \pm 0.04$  kpc for the Perseus arm and  $\text{Me } R_0 - R_0 = -0.08 \pm 0.03$  kpc for the Scutum arm.

The  $R_{0,\text{corr}}$  estimates obtained in Subsection 3.3 for the Perseus and Scutum arms (Table 4) were corrected for the systematic error found by the Monte Carlo technique, which led to the point estimates  $R_0 = 9.02$  and  $R_0 = 8.70$  kpc for the Perseus and Scutum arms, respectively. As the final estimate obtained by applying the three-point method to masers we took the weighted mean of these two values:

$$\langle R_0 \rangle = (w_1 \cdot 9.02 + w_2 \cdot 8.70) / (w_1 + w_2) = 8.8 \text{ kpc.} \quad (22)$$

Here, the weights  $w_1 = 1/(1.50^2 + 0.08^2)$  and  $w_2 = 1/(1.32^2 + 0.06^2)$  take into account the lengths of the confidence intervals for the two initial estimates (the boundaries of the intervals were determined as the order statistics of the set of values obtained by the Monte Carlo technique for  $N_{\text{MC}} = 1000$  catalogues) and their biases. The uncertainty of the final estimate was found as the mean error of the weighted mean before adjustment (Agekyan 1972):

$$\sigma_{\langle R_0 \rangle} = (2\sqrt{w_1 + w_2})^{-1} = 0.5 \text{ kpc.} \quad (23)$$

The parameters of the spiral arm segments were estimated by the two-point method at fixed  $R_0 = 8.8$  kpc (Table 6). To construct the model spiral approximating the nominal distribution of masers, we applied no jackknife corrections here. The difference in  $i$ ,  $\lambda_0$ , and  $(\sigma_w)_{\text{obs}}$  at  $R_0 = 8.8$  and 8.44 kpc (Table 5) is attributable to the correlation of these parameters with  $R_0$  (Table 7). Table 7 gives the linear correlation coefficients  $\kappa(p_1, p_2)$  for the Perseus and Scutum arms and the probability  $P_\kappa \equiv P(|\kappa| > |\kappa(p_1, p_2)|)$  to obtain a correlation coefficient greater in absolute value than the measured  $|\kappa(p_1, p_2)|$  in the absence of a correlation between the random variables  $p_1$  and  $p_2$  (Press et al. 1997). These quantities were determined through Monte Carlo simulations for the above model spirals at  $R_0 = 8.44$  kpc. All probabilities  $P_\kappa$  were found to be less than 0.05, i.e., all coefficients  $\kappa$  in Table 7 are significant. In most cases, the correlation between the parameters is moderate, except for some pairs of parameters including  $\lambda_0$ .

For all five segments Fig. 13 presents the model spirals with the parameters from Table 6 and the distribution of masers assigned to these segments in projection onto the Galactic plane. The contours of the Galactic bar in Fig. 13 are given for an ellipsoidal model with semiaxes 3.14 : 1.178 : 0.81 kpc and a position angle  $\varphi = 20^\circ$  (Casetti-Dinescu et al. 2013; Jilková et al. 2012).

## 5. DISCUSSION

The three-point method is similar in principle of generalization of *particular* solutions for  $R_0$ , in our case, obtained from triplets of objects, to the method of Feast and Shuttleworth (1965) within a different, kinematic, approach to determining  $R_0$ . The Feast–Shuttleworth method, which suggests the construction and analysis of the distribution function of individual  $R_0$  estimates based on *individual* objects, was previously quite

**Table 7.** Linear correlation coefficients  $\kappa(p_1, p_2)$  for the spiral segment parameters derived by the Monte Carlo technique for the Perseus and Scutum arms

$(p_1, p_2)$	$(R_0, i)$	$(R_0, \lambda_0)$	$(R_0, (\sigma_w)_{\text{obs}})$	$(i, \lambda_0)$	$(i, (\sigma_w)_{\text{obs}})$	$(\lambda_0, (\sigma_w)_{\text{obs}})$
Perseus arm						
$\kappa(p_1, p_2)$	-0.421	-0.738	-0.545	0.735	-0.063	0.514
$P_\kappa$	$6.41 \cdot 10^{-4}$	$1.17 \cdot 10^{-3}$	$7.97 \cdot 10^{-4}$	$1.16 \cdot 10^{-3}$	0.0466	$7.54 \cdot 10^{-4}$
Scutum arm						
$\kappa(p_1, p_2)$	-0.469	+0.437	-0.300	-0.843	-0.344	0.311
$P_\kappa$	$6.97 \cdot 10^{-4}$	$6.59 \cdot 10^{-4}$	$5.15 \cdot 10^{-4}$	$1.57 \cdot 10^{-3}$	$5.59 \cdot 10^{-4}$	$5.26 \cdot 10^{-4}$

$P_\kappa \equiv P(|\kappa| > |\kappa(p_1, p_2)|)$  is the probability in the case of null hypothesis to obtain a correlation coefficient greater in absolute value than the measured  $|\kappa(p_1, p_2)|$  for a pair of parameters  $(p_1, p_2)$ .

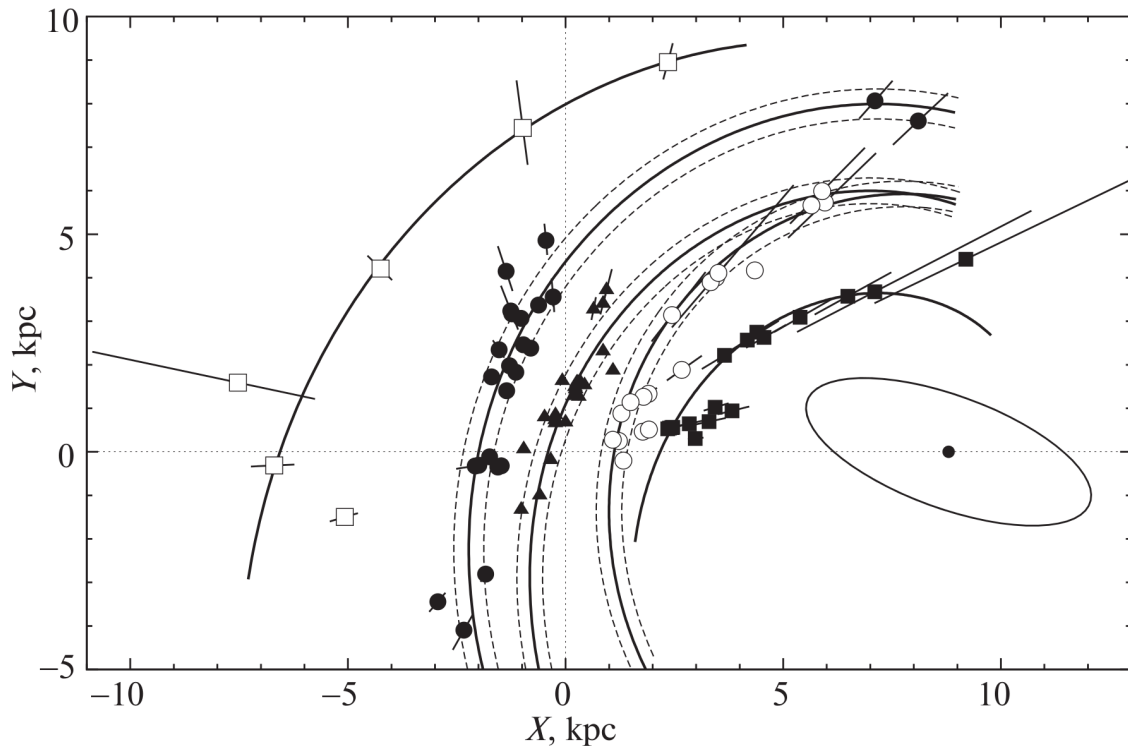


**Fig. 13.** The model spirals (solid lines) and the maser positions in projection onto the Galactic plane for the Outer (open squares), Perseus (filled circles), Local (filled triangles), Sagittarius (open circles), and Scutum (filled squares) arms at  $R_0 = 8.8$  kpc. The error bars reflect the parallax uncertainty. The natural scatter across the arms  $[\pm(\sigma_w)_0]$  relative to the models is indicated by the dashed lines for segments with  $(\sigma_w)_0^2 > 0$ . The ellipse indicates the Galactic bar; the circle at its center indicates the Galactic center.

popular (Balona and Feast 1974; Crampton et al. 1976; Loktin 1979). Such simplified methods are less efficient in the probabilistic sense than the simultaneous solution of the parameter optimization problem from all sample objects, but they allow one to show easily and clearly that the approach is operable and to judge the existence of a solution and its

quality. Therefore, applying such methods is quite justified at a certain stage of using a particular approach, especially if it is new. For example, in the next paper we are going to investigate some properties of the estimates for the distances to the pole of spiral arms by the three-point method. However, a method based on the search for an extremum of the target function should, of course, be developed in future for the proposed approach.

Note that the least-squares method (LSM) cannot be such a method, because it is not proper enough for this problem. For example, in the popular case of applying the LSM for optimization in the  $(\Lambda, \ln R/R_0)$  plane, none of the coordinates of the latter is a directly measurable quantity or argument, because the heliocentric distance characteristic, in the case of masers, this is the trigonometric parallax  $\varpi$ , is a measurable (with an error) quantity ( $l$  and  $b$  in this problem may be deemed errorless). The value of  $\varpi$  determines at once both  $\ln R/R_0$  and  $\Lambda$ . This makes the latter two quantities correlated differently, depending on the object’s position. The scatter of objects across the arm also leads to a similar (also complex) correlation between  $\ln R/R_0$  and  $\Lambda$ . These correlations are difficult to take into account, if at all possible. It is reasonable to assume the parallaxes  $\varpi$  (they are measured) and the deviation of an object from the spiral model in the configuration space (in the  $XY$  plane) to be normally distributed. There is no reason to assume  $\ln R/R_0$  and  $\Lambda$  to be normally distributed quantities, as suggested in the LSM, nor is there reason to consider some of these variables to be errorless. In principle, the LSM can be used to optimize the deviations from the spiral model in the  $XY$  plane. However, on the one hand, this leads to a sharp complication of the calculations and, on the other hand, this will still be insufficient, because the LSM disregards the errors in the distances (in  $\varpi$ ). The latter cannot be ignored: they are often significant and affect differently the result, depending on the object’s position (Fig. 13). These two types of scatter can be properly taken into account only within the maximum likelihood method, although this variant is more complex and laborious. We are working in this direction.

$R_0 = 8.8 \pm 0.5$  kpc found in this paper exceeds the recent mean (“best”) estimates of this parameter  $\langle R_0 \rangle_{\text{best}} = (7.9 \div 8.3) \pm (0.1 \div 0.4)$  kpc (Genzel et al. 2010; Foster and Cooper 2010; Nikiforov and Smirnova 2013; Bland-Hawthorn and Gerhard 2016; de Grijs and Bono 2016), but it is within the interval covered by the point estimates of  $R_0$  in modern publications. For example, Do et al. (2013) obtained  $R_0 = 8.92^{+0.58}_{-0.55}$  kpc through three-dimensional Jeans modeling (within the statistical parallax method) of the stellar kinematics of the Galactic nuclear star cluster; Catchpole et al. (2016) deduced a similar estimate,  $R_0 = 8.9 \pm \sim 0.4$  kpc, from Mira variables in the bulge. Given the errors, our result from the geometry of spiral segments is consistent with the estimate  $R_0 = 8.34 \pm 0.16$  kpc from the kinematics of masers based on the same database (Reid et al. 2014).

The  $i$  estimates in Table 6 confirm the difference between different spiral arms in pitch angle found by Reid et al. (2014). According to our results, this difference is significant when comparing the Scutum and Outer arms, on the one hand, and the Sagittarius and Perseus arms, on the other hand. An extrapolation of the model spiral of the Local arm shows that it can be a trailing branch of the Sagittarius arm (Fig. 13), at least on the basis of masers. This variant was not considered in Xu et al. (2013) devoted to the nature



of the Local arm.

In the case of segments with the most reliable solutions (the Perseus and Sagittarius arms),  $R_0$  affects noticeably the  $i$  estimate (cf. Tables 5 and 6) in accordance with the correlation coefficients (Table 7). This should be kept in mind when discussing the results of various pitch angle measurements for the Galactic spiral arms.

The natural scatters  $(\sigma_w)_0$  of masers across the Sagittarius, Local, and Perseus arms were found to be close to those found by Reid et al. (2014). However, for the Scutum and Outer arms, the farthest ones from the Sun among those revealed by these data, the variance  $(\sigma_w)_0^2$  turned out to be negative in all variants of calculations. This may imply that the parallax uncertainties given by Reid et al. (2014) for the masers of these two arms were overestimated. An alternative reason can be the selection effects when choosing the masers for the samples of these arms. For example, the Scutum sample consists of two groups inhomogeneous in  $(\sigma_w)_{\text{obs}}$  (and in parallax errors), one of which (at small  $l$ ) lies at a large angle to the spiral segment and has a significant scatter relative to it, while the other group is located in a direction almost tangential to the segment ( $l \sim 30^\circ$ ), in a narrow interval of  $l$ , which leads to a scatter across the segment much smaller than that for the first group.

Note that the assumption (number 5 in our list in the Introduction) about the coincidence between the pole of the spiral arms (in a more general case, the geometric center of the spiral pattern) and the Galactic center is currently a standard one in the parametric modeling of the Galactic spiral structure (see the review of Efremov (2011) and the papers on the spiral structure mentioned in the Introduction). At present, this assumption seems reasonable, because it is consistent with the observations of external spiral galaxies (see, e.g., Savchenko and Reshetnikov 2013), the numerical experiments (e.g., Korchagin et al. 2016), and the present views that the inner Galaxy is a dynamically "relaxed" system whose differently determined "centers" (the greatest star density or a different central feature of the spatial distribution, the central object, the barycenter, and others) virtually coincide (Bland-Hawthorn and Gerhard 2016). The currently available data are not yet accurate enough to directly establish the extent to which these centers coincide with one another and with the geometric center of the spiral structure introduced by us, but such problems should be kept in mind in future. Note separately that we do not use the assumption that the spiral arm extends to the very center of the Galaxy, considering the latter as the pole of the approximating spiral of the observed segment. The existence of a real arm only outside the Galactic bar or even in a limited interval of radii  $R$  is not a hindrance in using this approach.

## 6. CONCLUSIONS

We proposed a new approach to the spatial modeling of Galactic spiral arm segments that includes the determination of the distance to the pole of the spiral structure, i.e., the distance to the Galactic center  $R_0$ . To study the capabilities of this approach, we considered the problem of reconstructing the parameters of a logarithmic spiral as a geometric figure from points belonging to it by assuming the direction to the spiral pole to be

known and the points to represent a segment constituting less than one spiral turn. Our numerical–analytical study using the representative spirals for the Perseus and Scutum arms as examples leads us to the following conclusions.

- (1) Knowing the positions of four points of the segment uniquely solves the problem of reconstructing the spiral arm parameters. However, this solution cannot be used in practice: for any small change in the positions of the points the solution ceases to exist, because the spiral that passes through four arbitrary points in one turn generally does not exist.
- (2) If the positions of three points of the segment are known, then the solution exists always, but it is generally nonunique: apart from the initial  $R_0$ , there can be one or two additional roots. In this case,
  - (a) if the segment lies completely on one side of the  $X$  axis (the Galactic center–anticenter line) or touches the extreme point of this axis, then there are always two roots;
  - (b) if the segment crosses the  $X$  axis, then the root is usually unique, except for the segments that lie *almost* completely on one side of the  $X$  axis (three roots, two at the bifurcation points) and the short segments with most of their length being at negative longitudes  $l$ ,  $\Lambda$  (two roots);
  - (c) the additional roots usually differ greatly from the initial  $R_0$  (they are often negative for the Perseus arm) and are distinguishable from it by the pitch angle, except for the cases where the middle point of the segment is near the traverse directions ( $\Lambda_2 \approx$  from  $-80^\circ$  to  $-70^\circ$  and  $\Lambda_2 \approx$  from  $+100^\circ$  to  $+115^\circ$ );
  - (d) the region of configurations of triplets of points for which a unique solution exists is not small and corresponds to the segments in the solar sector of the Galaxy that are usually revealed by tracers with reliable distances.

This, three-point, method can be applied to real data and in numerical experiments provided that a criterion for choosing between the roots is introduced.

- (3) The segments that cross the  $X$  axis but are not centered near the traverse directions are preferred when seeking a geometrically exact solution and, probably, an approximation solution.

Based on the three-point method, we constructed a simplified algorithm for determining the parameters of a spiral segment from real objects. Applying the algorithm to the data from Reid et al. (2014) on masers with trigonometric parallaxes confirmed that, on the whole, the new approach is operable. We managed to obtain reliable solutions for the Perseus and Scutum arms. Averaging these results with the corrections for the sample finiteness and the estimator bias led to the final estimate of  $R_0 = 8.8 \pm 0.5$  kpc from the geometry of the spiral segments traced by masers.

We estimated the parameters of five spiral arm segments revealed by masers by a similar, two-point at fixed  $R_0$ , method. We confirmed that the pitch angles for different

spiral arms are generally different. Our results suggest that the Local arm can be a branch of the Sagittarius arm. We found a significant negative correlation between the pitch angle  $i$  and  $R_0$ . We showed that the observed scatter of masers relative to the Outer and Scutum arms could generally be explained by the catalogue uncertainties in the trigonometric parallaxes.

## ACKNOWLEDGMENTS

We are grateful to the referees for their useful remarks. This work was financially supported by the St. Petersburg State University (grant no. 6.37.341.2015).

## REFERENCES

1. T. A. Agekyan, *Fundamentals of the Error Theory for Astronomers and Physicists* (Nauka, Moscow, 1972) [in Russian].
2. V. S. Avedisova, *Sov. Astron. Lett.* **11**, 185 (1985).
3. L. A. Balona and M. W. Feast, *Mon. Not. R. Astron. Soc.* **167**, 621 (1974).
4. J. Bland-Hawthorn and O. Gerhard, *Ann. Rev. Astron. Astrophys.* **54**, 529 (2016).
5. V. V. Bobylev and A. T. Bajkova, *Astron. Lett.* **39**, 759 (2013).
6. V. V. Bobylev and A. T. Bajkova, *Mon. Not. R. Astron. Soc.* **437**, 1549 (2014).
7. D. I. Casetti-Dinescu, T. M. Girard, L. Jílková, et al., *Astron. J.* **146**, 33 (2013).
8. R. M. Catchpole, P. A. Whitelock, M. W. Feast, S. M. G. Hughes, M. Irwin, and C. Alard, *Mon. Not. R. Astron. Soc.* **455**, 2216 (2016).
9. D. Crampton, D. Bernard, B. L. Harris, and A. D. Thackeray, *Mon. Not. R. Astron. Soc.* **176**, 683 (1976).
10. A. K. Dambis, L. N. Berdnikov, Yu. N. Efremov, A. Yu. Kniazev, A. S. Rastorguev, E. V. Glushkova, V. V. Kravtsov, D. G. Turner, et al., *Astron. Lett.* **41**, 489 (2015).
11. T. M. Dame, B. G. Elmegreen, R. S. Cohen, and P. Thaddeus, *Astrophys. J.* **305**, 892 (1986).
12. T. Do, G. D. Martinez, S. Yelda, A. Ghez, J. Bullock, M. Kaplinghat, J. R. Lu, A. H. G. Peter, et al., *Astrophys. J.* **779**, L6 (2013).
13. Yu. N. Efremov, *Astron. Rep.* **55**, 108 (2011).
14. B. Efron and C. Stein, *Ann. Statistics* **9**, 586 (1981).
15. M. W. Feast and M. Shuttleworth, *Mon. Not. R. Astron. Soc.* **130**, 245 (1965).

16. T. Foster and B. Cooper, *ASP Conf. Ser.* **438**, 16 (2010).
17. C. Francis and E. Anderson, *Mon. Not. R. Astron. Soc.* **422**, 1283 (2012).
18. R. Genzel, F. Eisenhauer, and S. Gillessen, *Rev. Mod. Phys.* **82**, 3121 (2010).
19. D. A. Grabelsky, R. S. Cohen, L. Bronfman, and P. Thaddeus, *Astrophys. J.* **331**, 181 (1988).
20. R. de Grijs and G. Bono, *Astrophys. J. Suppl. Ser.* **227**, 5 (2016).
21. L. Jílková, G. Carraro, B. Jungwiert, and I. Minchev, *Astron. Astrophys.* **541**, A64 (2012).
22. A. I. Kobzar', *Applied Mathematical Statistics for Engineers and Scientists* (Fizmatlit, Moscow, 2006) [in Russian].
23. V. I. Korchagin, S. A. Khoperskov, and A. V. Khoperskov, *Baltic Astron.* **25**, 356 (2016).
24. A. V. Loktin, *Sov. Astron.* **23**, 671 (1979).
25. I. I. Nikiforov, *ASP Conf. Ser.* **316**, 199 (2004).
26. I. I. Nikiforov and E. E. Kazakevich, *Izv. GAO* **219**, 245 (2009).
27. I. I. Nikiforov and O. V. Smirnova, *Astron. Nachr.* **334**, 749 (2013).
28. I. I. Nikiforov and T. V. Shekhovtsova, in *Stellar Dynamics: From Classic to Modern, Proceedings of the International Conference, St. Petersburg, Russia, Aug. 21–27, 2000*, Ed. by L. P. Ossipkov and I. I. Nikiforov (Saint Petersburg Univ. Press, St. Petersburg, 2001), p. 28.
29. E. D. Pavlovskaya and A. A. Suchkov, *Sov. Astron.* **28**, 389 (1984).
30. M. Pohl, P. Englmaier, and N. Bissantz, *Astrophys. J.* **677**, 283 (2008).
31. M. E. Popova, *Astron. Lett.* **32**, 244 (2006).
32. M. E. Popova and A. V. Loktin, *Astron. Lett.* **31**, 171 (2005).
33. W. H. Press, S. A. Teukolsky, W. T. Vetterling, and B. P. Flannery, *Numerical Recipes in C* (Cambridge Univ. Press, Cambridge, UK, 1997).
34. M. H. Quenouille, *Ann. Math. Statistics* **20**, 355 (1949).
35. M. H. Quenouille, *Biometrika* **43**, 353 (1956).
36. M. J. Reid, K. M. Menten, X. W. Zheng, A. Brunthaler, L. Moscadelli, Y. Xu, B. Zhang, M. Sato, et al., *Astrophys. J.* **700**, 137 (2009).

37. M. J. Reid, K. M. Menten, A. Brunthaler, X. W. Zheng, T. M. Dame, Y. Xu, Y. Wu, B. Zhang, et al., *Astrophys. J.* **783**, 130 (2014).
38. S. S. Savchenko and V. P. Reshetnikov, *Mon. Not. R. Astron. Soc.* **436**, 1074 (2013).
39. J. P. Vallée, *Astron. J.* **95**, 750 (1988).
40. Y. Xu, J. J. Li, M. J. Reid, K. M. Menten, X. W. Zheng, A. Brunthaler, L. Moscadelli, T. M. Dame, et al., *Astrophys. J.* **769**, 15 (2013).

## APPENDIX

### *A1. Determining the Confidence Region for the Model Spiral Found by the Three-Point Method*

The  $1\sigma$  confidence region for the model spiral was determined using the following algorithm. We fixed the ray  $C_0M$  emerging from the pole  $C_0$  of the model spiral at an angle  $\Lambda$  to the  $X$  axis (Fig. 14a). For a given  $\Lambda$  we determined the points of intersection  $P_j$  of the ray  $C_0M$  with each of the  $N_{\text{sol}}$  spirals obtained from triplets of masers  $M_{1,j}$ ,  $M_{2,j}$ ,  $M_{3,j}$ .

Let us derive the equation to find the longitude  $\lambda_j$  of the point of intersection  $P_j(X_{P_j}, Y_{P_j})$  of the spiral and the ray with its origin on the  $X$  axis. For point  $P_j$  belonging to a spiral with parameters  $R_{0,j}$ ,  $k_j$ , and  $\lambda_{0,j}$  the following equalities are valid:

$$\begin{aligned} R(\lambda_j) &= |R_{0,j}|e^{k_j(\lambda_j - \lambda_{0,j})}, \\ X_{P_j} &= R_{0,j} - R(\lambda_j) \cos \lambda_j, \\ Y_{P_j} &= R(\lambda_j) \sin \lambda_j \end{aligned} \tag{24}$$

(see Eqs. (3) and (6)). The equation of the straight line  $C_0M$  in Cartesian coordinates is

$$Y = (\text{Me } R_0 - X) \tan \Lambda. \tag{25}$$

Substituting Eq. (24) for the coordinates  $X_{P_j}$  and  $Y_{P_j}$  into (25) gives the equality

$$R(\lambda_j) \sin \lambda_j = [\text{Me } R_0 - R_{0,j} + R(\lambda_j) \cos \lambda_j] \tan \Lambda, \tag{26}$$

which is valid for point  $P_j$  as the intersection of the spiral and the straight line. Taking into account Eq. (24) for  $R(\lambda_j)$ , we finally obtain the equation for the longitude  $\lambda_j$  of the sought-for point  $P_j$

$$|R_{0,j}|e^{k_j(\lambda_j - \lambda_{0,j})} \sin \lambda_j - [\text{Me } R_0 - R_{0,j} + |R_{0,j}|e^{k_j(\lambda_j - \lambda_{0,j})} \cos \lambda_j] \tan \Lambda = 0. \tag{27}$$

The roots of Eq. (27) were calculated in the segment  $\lambda_j \in [-\pi; \pi)$ . From the two formal roots we chose the root whose sign coincided with the sign of  $\Lambda$ . The quantity  $\lambda_j$  defines point  $P_j$  of Eqs. (24).

For fixed  $\Lambda$  we found the median of the set of distances  $\{R_j\}_{j=1}^{N_{\text{sol}}}$ , where  $R_j = |C_0P_j|$ , and two quantiles of the  $R_j$  distribution measured from the median on different sides of it and containing together a fraction of the distribution for the  $1\sigma$  confidence level, i.e.,  $\frac{\approx 68.3\%}{2}$  in each quantile. The outer boundaries of the quantiles were taken as the boundaries of the confidence interval for the model quantity  $R(\Lambda)$  defined by the model spiral for a given  $\Lambda$  (Fig. 14b). Solving the same problem for various values of  $\Lambda$  allows the boundaries of the confidence region to be found for a model spiral with any resolution in  $\Lambda$  (Fig. 14b, see also Fig. 7).

*A2. Estimating the Natural Root-Mean-Square Scatter of Masers  
Across the Spiral Segment*

Let  $M_j$  be the nominal position of a maser in accordance with the measurements,  $\varpi_j$  and  $\sigma_{\varpi_j}$  be, respectively, the parallax of the maser and its uncertainty given in the catalogue. Here,  $j = 1, 2, \dots, N$ , where  $N$  is the size of the sample of masers assigned to a given segment. Let us introduce the following notation for the distances from the points on the line of sight to the feet of the perpendiculars drawn through these points to the spiral (Fig. 15a):

$$\begin{aligned} \rho_j &= |M_jO_j|, & |M_jS| &= \varpi_j^{-1}, \\ \rho_{j,1} &= |M'_jO'_j|, & |M'_jS| &= (\varpi_j - \sigma_{\varpi_j})^{-1}, \\ \rho_{j,2} &= |M''_jO''_j|, & |M''_jS| &= (\varpi_j + \sigma_{\varpi_j})^{-1}. \end{aligned} \quad (28)$$

Here,  $O_j$ ,  $O'_j$ , and  $O''_j$  are the foot points of the perpendiculars determined by the positions of points  $M_j$ ,  $M'_j$ , and  $M''_j$  on the line of sight, respectively;  $S$  is the position of the Sun.

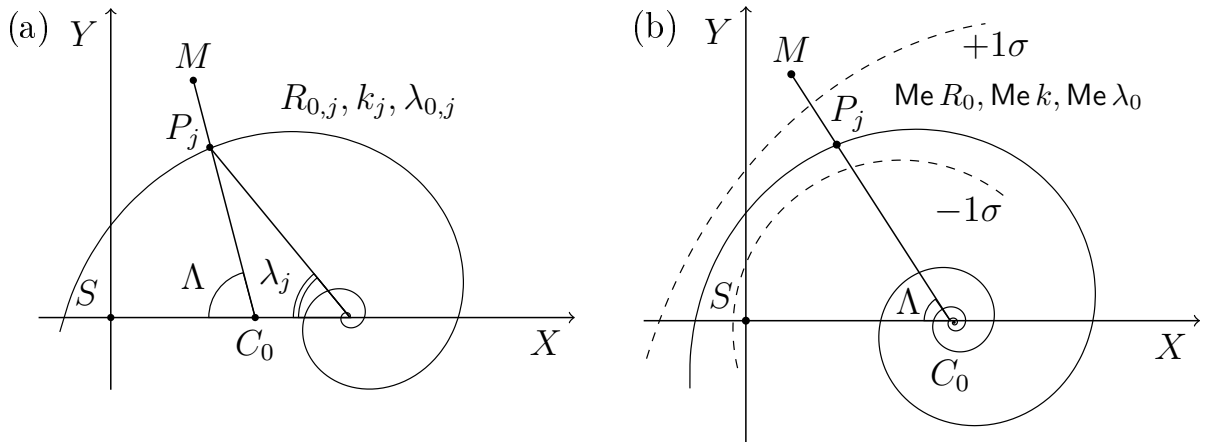


**Fig. 14.** (a) To the derivation of the equation for finding the longitude  $\lambda_j$  of the point of intersection  $P_j$  of a spiral with parameters  $R_{0,j}, k_j, \lambda_{0,j}$  and the ray  $C_0M$ . (b) To the determination of the confidence region for a model spiral with parameters  $Me R_0, Me k, Me \lambda_0$ ; the dashed lines mark the boundaries of this region for the  $1\sigma$  confidence level; the highlighted segment on the ray  $C_0M$  indicates the confidence interval for a model value of  $R$  at fixed  $\Lambda$ .  $C_0$  is the pole of the model spiral and  $S$  is the position of the Sun.

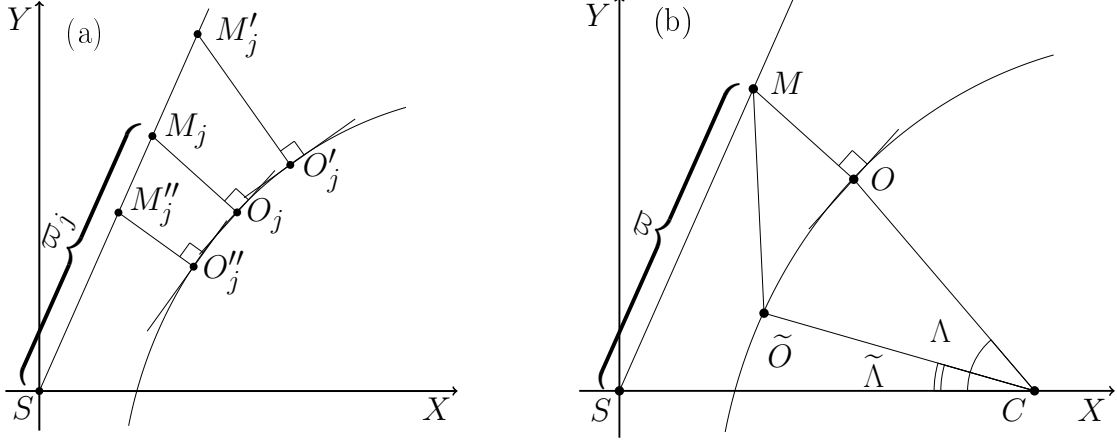


**Fig. 15.** (a) To the determination of the scatter across the spiral arm segment. (b) To the determination of the distance from a point ( $M$ ) to the spiral.  $S$  is the position of the Sun,  $C$  is the spiral pole.

Knowing the distances (28) allows us to obtain the following estimates for the observed variance of objects across the spiral arm segment,  $(\sigma_w)_{\text{obs}}^2$ , the contribution of the uncertainties in the parallaxes to this variance,  $(\sigma_w)_{\varpi}^2$ , and the natural variance of objects across the segment,  $(\sigma_w)_0^2$ :

$$(\sigma_w)_{\text{obs}}^2 = \frac{1}{N-3} \sum_{j=1}^N \rho_j^2, \quad (29)$$

$$(\sigma_w)_{\varpi}^2 = \frac{1}{N-3} \left[ \sum_{j=1}^N \frac{(\rho_j - \rho_{j,1})^2 + (\rho_j - \rho_{j,2})^2}{2} \right], \quad (30)$$

$$(\sigma_w)_0^2 = (\sigma_w)_{\text{obs}}^2 - (\sigma_w)_{\varpi}^2. \quad (31)$$

The distances (28) from the points to the spiral were calculated as follows. Let  $(X_0, Y_0)$  be the Cartesian coordinates of point  $M$ ;  $\tilde{O}(\tilde{X}, \tilde{Y})$  be an arbitrary point of the spiral with a nominal Galactocentric longitude  $\tilde{\Lambda}$ ;  $R_0$ ,  $k$ , and  $\lambda_0$  be the spiral parameters. We found such a value of the longitude  $\Lambda$  at which the distance  $|M\tilde{O}|(\tilde{\Lambda} = \Lambda)$  was smallest (Fig. 15b).

Let us express the coordinates of point  $\tilde{O}$  via  $\tilde{\Lambda}$  and the spiral parameters:

$$\tilde{X} = R_0 - |R_0|e^{k(\tilde{\Lambda}-\lambda_0)} \cos \tilde{\Lambda}, \quad (32)$$

$$\tilde{Y} = |R_0|e^{k(\tilde{\Lambda}-\lambda_0)} \sin \tilde{\Lambda}. \quad (33)$$

Let us find the value of  $\Lambda$  that provides the minimum of the function

$$F(\tilde{\Lambda}) \equiv |M\tilde{O}|^2 = [\tilde{X}(\tilde{\Lambda}) - X_0]^2 + [\tilde{Y}(\tilde{\Lambda}) - Y_0]^2. \quad (34)$$

After taking the derivative  $F'(\tilde{\Lambda})$ , we obtain the equation to determine  $\Lambda$ :

$$(X_0 - R_0) (\sin \Lambda - k \cos \Lambda) + Y_0 (k \sin \Lambda + \cos \Lambda) - k|R_0|e^{k(\Lambda-\lambda_0)} = 0. \quad (35)$$

Having numerically determined the roots  $\Lambda$  of Eq. (35) on the spiral turn  $-\pi \leq \tilde{\Lambda} < \pi$ , we calculate the corresponding values of  $F(\Lambda)$ . Since there exist two extrema of  $F(\tilde{\Lambda})$  on the spiral turn, the smallest of the two values of  $\sqrt{F(\tilde{\Lambda})}$  is the sought-for distance.

### A3. The Jackknife Technique

The jackknife technique is used to estimate the variance and bias of the estimator (statistical estimate) for a parameter (Quenouille 1949, 1956; Efron and Stein 1981). We mean the bias due to the sample finiteness. Below we give the formulas of the technique as applied to the median estimate  $\text{Me } R_0$  by the three-point method as to the estimator.

Let the median  $\text{Me } R_0$  be found from the set of triplets formed from a sample of  $N$  objects. Consider  $N$  subsamples ( $N - 1$  in size each) such that the  $p$ th object of the original sample is absent in subsample  $p$ . For each of the subsamples from all the selected triplets of its objects we will determine the median  $(\text{Me } R_0)_p$ ,  $p = 1, 2, \dots, N$ . Next, we will calculate the arithmetic mean of  $(\text{Me } R_0)_p$

$$\langle \text{Me } R_0 \rangle_J = \frac{1}{N} \sum_{p=1}^N (\text{Me } R_0)_p. \quad (36)$$

The variance of the three-point estimate  $\text{Me } R_0$  as an estimator is then

$$\sigma_{R_0, J}^2 = \frac{N-1}{N} \sum_{p=1}^N [(\text{Me } R_0)_p - \langle \text{Me } R_0 \rangle_J]^2, \quad (37)$$

while the corrected value of this estimate is

$$R_{0, \text{corr}} = N \text{Me } R_0 - (N-1) \langle \text{Me } R_0 \rangle_J. \quad (38)$$

The estimator bias is given by the difference  $\text{Me } R_0 - R_{0, \text{corr}}$ ; the correction to the estimate is a bias with the opposite sign:

$$\Delta R_0 = R_{0, \text{corr}} - \text{Me } R_0. \quad (39)$$